The Astrophysical Journal, 821:98 (18pp), 2016 April 20 doi:10.3847/0004-637X/821/2/98

THE JCMT GOULD BELT SURVEY: DENSE CORE CLUSTERS IN ORION B

H. Kirk[1], D. Johnstone[1,2,3], J. Di Francesco[1,2], J. Lane[2], J. Buckle[4,5], D. S. Berry[3], H. Broekhoven-Fiene[2], M. J. Currie[3], M. Fich[6], J. Hatchell[7], T. Jenness[3,8], J. C. Mottram[9,10], D. Nutter[11], K. Pattle[12], J. E. Pineda[13,14,15], C. Quinn[10], C. Salji[4,5], S. Tisi[6], M. R. Hogerheijde[9], and D. Ward-Thompson[12]
The JCMT Gould Belt Survey team[16]
[1] NRC Herzberg Astronomy and Astrophysics, 5071 West Saanich Road, Victoria, BC, V9E 2E7, Canada
[2] Department of Physics and Astronomy, University of Victoria, Victoria, BC, V8P 1A1, Canada
[3] Joint Astronomy Centre, 660 N. A'ohōkū Place, University Park, Hilo, HI 96720, USA
[4] Astrophysics Group, Cavendish Laboratory, J J Thomson Avenue, Cambridge, CB3 0HE, UK
[5] Kavli Institute for Cosmology, Institute of Astronomy, University of Cambridge, Madingley Road, Cambridge, CB3 0HA, UK
[6] Department of Physics and Astronomy, University of Waterloo, Waterloo, Ontario, N2L 3G1, Canada
[7] Physics and Astronomy, University of Exeter, Stocker Road, Exeter EX4 4QL, UK
[8] LSST Project Office, 933 N. Cherry Avenue, Tucson, AZ 85719, USA
[9] Leiden Observatory, Leiden University, P.O. Box 9513, 2300 RA Leiden, The Netherlands
[10] Max-Planck Institute for Astronomy, Königstuhl 17, D-69117 Heidelberg, Germany
[11] School of Physics and Astronomy, Cardiff University, The Parade, Cardiff, CF24 3AA, UK
[12] Jeremiah Horrocks Institute, University of Central Lancashire, Preston, Lancashire, PR1 2HE, UK
[13] European Southern Observatory (ESO), Garching, Germany
[14] Jodrell Bank Centre for Astrophysics, Alan Turing Building, School of Physics and Astronomy, University of Manchester, Oxford Road, Manchester, M13 9PL, UK
Received 2015 November 18; accepted 2016 January 29; published 2016 April 18

ABSTRACT

The James Clerk Maxwell Telescope Gould Belt Legacy Survey obtained SCUBA-2 observations of dense cores within three sub-regions of Orion B: LDN 1622, NGC 2023/2024, and NGC 2068/2071, all of which contain clusters of cores. We present an analysis of the clustering properties of these cores, including the two-point correlation function and Cartwright's Q parameter. We identify individual clusters of dense cores across all three regions using a minimal spanning tree technique, and find that in each cluster, the most massive cores tend to be centrally located. We also apply the independent M–Σ technique and find a strong correlation between core mass and the local surface density of cores. These two lines of evidence jointly suggest that some amount of mass segregation in clusters has happened already at the dense core stage.

Key words: stars: formation – submillimeter: ISM

1. INTRODUCTION

Most stars begin their lives within a clustered environment (e.g., Lada & Lada 2003; Porras et al. 2003), highlighting the importance of understanding this mode of star formation. Over the past decade, significant effort has been made to characterize the clustering properties of the youngest stellar clusters to aid in constraining theories of cluster formation and evolution. Studies of nearby young stellar clusters span a range of properties from very small and sparse systems (e.g., Kirk & Myers 2011) to denser and more populous systems (e.g., Gutermuth et al. 2009; Feigelson et al. 2013; Kuhn et al. 2014). Combining cluster catalogs with detailed modeling can inform a variety of topics including the timescale of the initial cluster formation (e.g., Tan et al. 2006; Parmentier et al. 2014), the presence of multiple generations of cluster formation and their geometries (e.g., Ellerbroek et al. 2013), the role of early sub-cluster merging in the appearance of present-day clusters (e.g., Moeckel & Bonnell 2009), and the effects of gas explusion and feedback on cluster formation and early evolution (e.g., Pfalzner & Kaczmarek 2013; Krumholz et al. 2014, p. 243).

A complementary approach to measuring the properties of young stellar systems is characterizing the properties of the dense gas and dust prior to and during the initial stages of cluster formation. A variety of studies also exist in this regime as well, characterizing the properties and stability of dense cores, the kinematic properties of core and cluster gas, the influence of outflows, and heating of cluster cores (see, for example Tafalla et al. 2006; Kirk et al. 2007; Wang et al. 2008; Foster et al. 2009; Friesen et al. 2009; Maruta et al. 2010; Csengeri et al. 2011; Palau et al. 2013; Pattle et al. 2015). In terms of characterizing the dust continuum properties of dense cores in clusters (such as distributions of their masses and positions), the James Clerk Maxwell Telescope (JCMT) Gould Belt Survey (GBS) can make a strong contribution. The JCMT GBS performed a uniform large-scale mapping of thermal dust emission at 850 and 450 μm of nearby molecular clouds (the Gould Belt) visible from the northern hemisphere (Ward-Thompson et al. 2007). These maps include catalogs of dense cores to be identified around many nearby cluster-forming regions including Orion A (Salji et al. 2015 and Mairs et al. 2016, in preparation), Orion B (Kirk et al. 2015), and Ophiuchus (Pattle et al. 2015). This extensive set of dense core catalogs allows for a uniform analysis of the clustering

[15] Current address: Max Planck Institute for Extraterrestrial Physics, Giessenbachstrasse 1, D-85748 Garching, Germany.
[16] The full members of the JCMT Gould Belt Survey Consortium are P. Bastien, D. S. Berry, D. Bresnahan, H. Broekhoven-Fiene, J. Buckle, H. Butner, M. Chen, A. Chrysostomou, S. Coude, M. J. Currie, C. J. Davis, E. Drabek-Maunder, A. Duarte-Cabral, J. Di Francesco, M. Fich, J. Fiege, P. Friberg, R. Friesen, G. A. Fuller, S. Graves, J. Greaves, J. Gregson, J. Hatchell, M. R. Hogerheijde, W. Holland, T. Jenness, D. Johnstone, G. Joncas, J.M. Kirk ,H. Kirk, L. B. G. Knee, S. Mairs, K. Marsh, B. C. Matthews, G. Moriarty-Schieven, J. C. Mottram, C. Mowat, K. Pattle, J. Rawlings, J. Richer, D. Robertson, E. Rosolowsky, D. Rumble, S. Sadavoy, N. Tothill, H. Thomas, S. Viti, D. Ward-Thompson, G. J. White, J. Wouterloot, J. Yates, and M. Zhu.

properties of dense cores, which can then provide other constraints on the initial conditions of clusters and the physical processes shaping their evolution. Our focus in the present analysis is on the clustered population within Orion B, a region known to harbour several active cluster-forming regions (e.g., Meyer et al. 2008).

One particularly controversial aspect of cluster formation is mass segregation, namely is it present, and if so, is it primordial? Difficulties arise in the measurement of mass segregation from a host of challenges including the definition of a cluster, the definition of mass segregation, and the effects of observational biases. The determination of primordiality is also fraught with additional complications which again include how clusters are defined, cluster age determination, and whether or not the present day cluster is the product of an earlier merger of smaller systems that has since dynamically relaxed. While ongoing innovative work can help to overcome these challenges, it is also possible to address the question from the other side of star formation: if some degree of mass segregation is apparent in dense cores before the onset of star formation, then this lends support to the idea of primordial mass segregation in young stellar clusters.

In this paper, we use two independent techniques to look for the presence of mass segregation within clusters of dense cores in the Orion B molecular cloud. We follow the initial characterization of dense cores in this region by Kirk et al. (2015), which is summarized in Section 2. In Section 3 we introduce the minimal spanning tree (MST), and with it we find a general tendency for the most massive dense core(s) of a cluster to lie near the cluster centre. In Section 4 we introduce the M–Σ technique, and with it we find more massive cores have a tendency to lie in zones of higher core–core surface density. In Section 5 we present additional measures of the clustering properties of the dense cores, including the two-point correlation function. In Section 6 we discuss our results and their implications for the broader picture of cluster formation.

2. OBSERVATIONS

Three separate regions within Orion B were observed with SCUBA-2 (Holland et al. 2013) at 850 and 450 μm as part of the JCMT GBS (Ward-Thompson et al. 2007): LDN 1622, NGC 2023/2024, and NGC 2068/2071. NGC 2024, NGC 2068, and NGC 2071 are the most vigorous sites of ongoing star formation in Orion B, representing 60%–90% of its current young stellar objects (YSOs) (e.g., Lada et al. 1991; Meyer et al. 2008). The SCUBA-2 observations span a generous area around these three clustered star-forming regions, as well as several less prominent ones, with total areal coverages of 0.6 deg^2, 2.1 deg^2, and 1.7 deg^2 around L1622, NGC 2023/2024, and NGC 2068/2071, respectively. Analysis of the SCUBA-2 maps was first presented in Kirk et al. (2016, hereafter K16), using the GBS Legacy Release 1 reduction methodology (see, e.g., Mairs et al. 2015). In brief, individual observations were reduced using the JCMT's standard Starlink software (see Chapin et al. 2013, for a description of *makemap*), and then mosaicked together. Smaller-scale sources (i.e., those of size below roughly 2.′5) are generally well-recovered in the final map, while larger-scale sources can be subject to some filtering (see K16 for more details). All of the Orion B maps and associated data products are available at https://doi.org/10.11570/16.0003.

K16 identified dense cores in the 850 μm map—using the *FellWalker* algorithm (Berry 2015), finding a total of 29 dense cores in L1622, 546 in NGC 2023/2024, and 322 in NGC 2068/2071. *FellWalker* effectively identifies cores based on local peaks of emission, defining their extents based on the locations at which local gradients in flux are directed toward the peak. As such, dense core boundaries are irregular, and each pixel in the map is assigned to a maximum of one core. Some of the dense cores identified are elongated—12% have ratios of 2 or higher in comparing their vertical and horizontal extents—but there is no indication in K16 that their other basic properties differ from the rest of the cores. In our present analysis, we treat all cores identically, regardless of their elongation. The robustness of individual cores is ensured through *FellWalker* criteria specifying a minimum spatial and flux separation between closely spaced peaks, a minimum core size larger than the telescope beam, and a minimum gradient and flux level for all pixels associated with the peak. Of the dense cores identified in the three regions, 5, 25, and 34, respectively, were classified as protostellar, based on a comparison with the *Spitzer*-based YSO catalog of Megeath et al. (2012) and the *Herschel*-based YSO catalog of Stutz et al. (2013), noting that the latter catalog covers a deep but limited area within Orion B. The minimum flux for a dense core to be identified was 7.4 mJy, which corresponds to a mass of $\sim$0.01 $M_\odot$, assuming a distance of 415 pc, a temperature of 20 K, and a dust opacity of 0.0125 g cm^{-2} at 850 μm (see K16 for details). For a star-forming region at a single distance with an invariant population of dust grains, the observed 850 μm flux is proportional to both the total amount of material present in the beam and its temperature. The assumption of a constant 20 K temperature is reasonable for the starless cores, but is likely to cause the mass to be overestimated for the protostellar cores by a factor of a few. For this reason, we separate the two populations of cores for some of our analysis here.

Comparing the mass within lower column density material, as measured by *Herschel* and *Planck* by Lombardi et al. (2014), K16 find that the NGC 2023/2024 and NGC 2068/2071 regions are likely in the process of forming several hundred protostars each, while L1622 harbours a more modest number of protostars and lacks the necessary dense material to be able to form significantly more.

In relating the results of our clustering analysis below to the initial conditions for protostellar clusters, we make several reasonable assumptions, which are discussed in more detail in Section 6.2 and Appendix B.2. While it is not necessary to assume that each core forms a single star, we do assume that similar cores will form similar groups of stars, regardless of their locations in the larger environment. Similarly, while we do not assume a one-to-one relationship between the masses of a dense core and a protostar, we do assume that the most massive cores are most likely to form the most massive protostars. It is possible that some of the dense cores in the K16 catalog will eventually disperse without forming any stars. These cores, however, are likely to be the least massive ones, which we find are the least likely to be associated with clustering. We note that K16 estimated that the majority of starless dense cores in Orion B are presently bound, due to a combination of self-gravity and pressure from the external weight of the ambient cloud material.

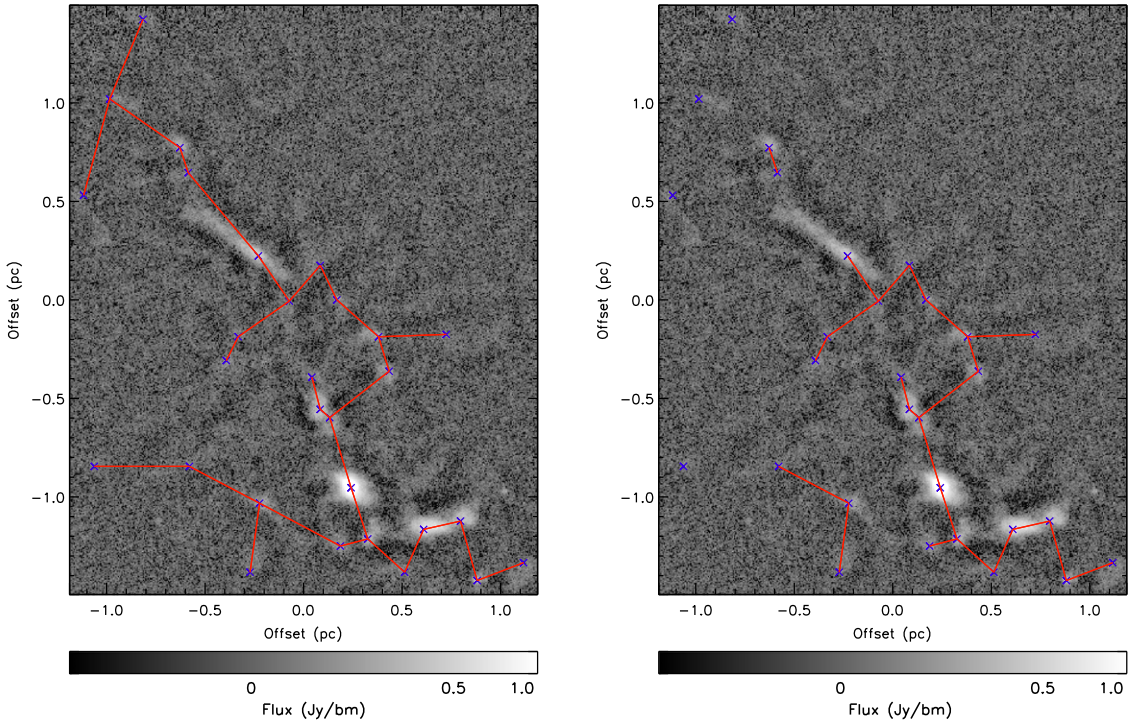

Figure 1. Minimal spanning tree structure for L1622. In both panels, the background grayscale image shows the SCUBA-2 850 μm emission (truncated to the extent over which dense cores were identified), while the blue crosses show the dense cores. In the left panel, the red lines show the entire original MST structure. In the right panel, branches longer than $L_{\rm crit}$ (0.42 pc) have been removed.

3. MST ANALYSIS

A visual examination of the three regions mapped in Orion B reveals clusters of dense cores, especially in the larger and more active NGC 2023/2024 and NGC 2068/2071 regions. We use a MST to identify these clusters to analyze their properties. MSTs have been used previously to identify clusters of stars (e.g., Gutermuth et al. 2009; Billot et al. 2011; Kirk & Myers 2011; Masiunas et al. 2012), and as a tool to compare simulations with observations (e.g., Kirk et al. 2014). An MST basically defines a structure in which all sources are connected by their minimum possible separations, i.e., branches. Within an MST structure, clusters are apparent as sets of points connected by short branches. We follow the method of Gutermuth et al. (2009, hereafter G09) to estimate $L_{\rm crit}$, the critical branch length, used to distinguish clustered from isolated sources. G09 found that young stellar clusters tend to have a characteristic distribution of branch lengths when plotted as cumulative number versus length: i.e., a steep, nearly linear rise at short branch lengths, followed by a turn-over to a shallow, nearly linear slope at the longest branch lengths. G09 defined $L_{\rm crit}$ as the intersection point between linear fits to the two ends of the distribution (see Figure 1 of G09). Sources which remain connected after all branches with lengths above $L_{\rm crit}$ are removed are considered clusters. In this manner, clusters are easily identified as local over-densities, rather than relying on a fixed surface density threshold. Kirk & Myers (2011, hereafter KM11) followed the same procedure as G09, setting the minimum number of YSOs for a cluster at 11 since fewer sources make the determination of cluster properties such as the centre position difficult. Here, as in KM11, the cluster centre is defined as the median position of cluster members.

We find that the cumulative branch length distribution of cores in each Orion B region follows a similar distribution, and so we apply the same cluster-identification method as in G09 and KM11, including the minimum number of cluster members (eleven) and centre position used in the latter analysis. Figures 1–3 show the full and chopped MST structures in L1622, NGC 2023/2024, and NGC 2068/2071 using the procedure described in KM11. The main clusters selected by this method correspond very well with how the eye would subdivide the region into clusters. In NGC 2023/2024 and NGC 2068/2071, multiple clusters are identified, while in L1622 only a single cluster is identified. In total, 69% (20/29), 71% (389/546), and 75% (243/322) cores were associated with a cluster in each of L1622, NGC 2023/2024, and NGC 2068/2071. We measure best-fit $L_{\rm crit}$ values of 0.42 pc (L1622), 0.26 pc (NGC 2023/2024), and 0.28 pc (NGC 2068/2071). Table 1 summarizes the properties of the clusters identified in all three regions, and each cluster is also shown in the A in Figures 10 and 11. A full examination of the effects of the uncertainty in $L_{\rm crit}$ on the cluster definitions and subsequent results is also given in Appendix A.

3.1. Offset Ratios

Figure 4 shows a zoomed-in view of the largest two clusters identified in NGC 2068/2071. In the figure, the size of the circle scales with the total flux of the dense core. The highest flux core (open yellow circle) tends to be relatively centrally located in both of the examples shown in Figure 4. We can quantify this tendency further, using a technique introduced by KM11. For each core in a cluster, we calculate its offset from the cluster centre. The ratio of the offset of the highest flux core to the median value of all of the core offsets gives an indication of how relatively close the core is to the cluster centre, with offset ratios less than one indicating a centrally located core. As might be naively expected, KM11 showed that clusters with

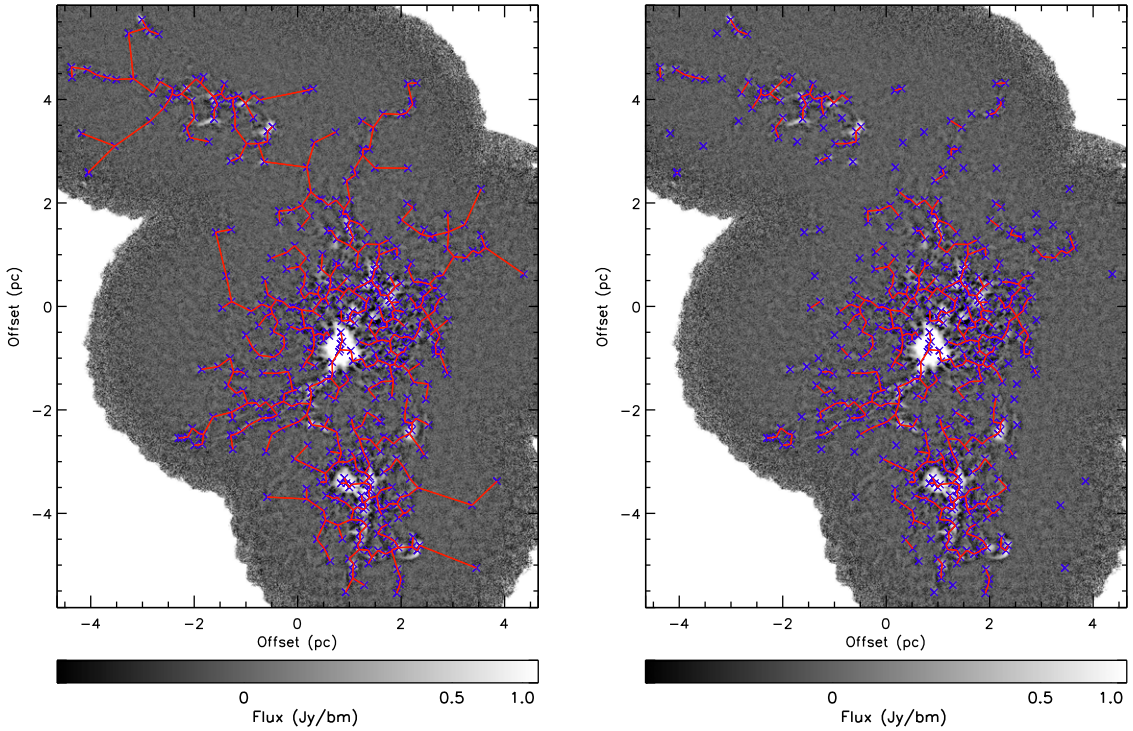

Figure 2. Minimal spanning tree structure for NGC 2023/2024. In both panels, the background grayscale image shows the SCUBA-2 850 μm emission (truncated to the extent over which dense cores were identified), while the blue crosses show the dense cores. In the left panel, the red lines show the entire original MST structure. In the right panel, branches longer than $L_{\rm crit}$ (0.26 pc) have been removed.

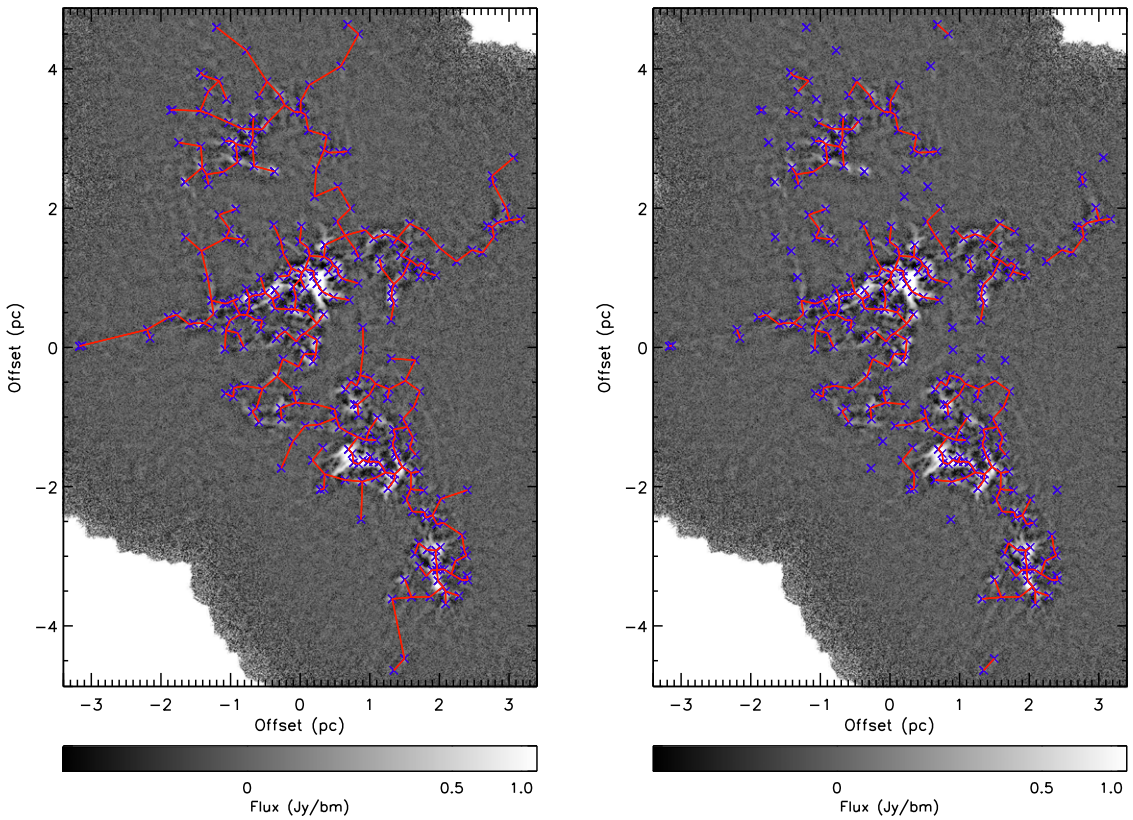

Figure 3. Minimal spanning tree structure for NGC 2068/2071. In both panels, the background grayscale image shows the SCUBA-2 850 μm emission (truncated to the extent over which dense cores were identified), while the blue crosses show the dense cores. In the left panel, the red lines show the entire original MST structure. In the right panel, branches longer than $L_{\rm crit}$ (0.28 pc) have been removed.

Table 1
Properties of MST-identified Clusters

Region	Index	N[a]	S_{max}[b] (Jy)	$S_{max,sl}$[b] (Jy)	S_{med}[b] (Jy)	S_{tot}[b] (Jy)	O_{max}[c] (pc)	$O_{max,sl}$[c] (pc)	O_{med}[c] (pc)	f_{proto}[d] (%)
LDN 1622	1	20	4.89	1.71	0.17	12.23	0.48	0.83	0.63	25.0
NGC 2023/2024	1	259	119.52	5.34	0.17	420.96	0.58	0.86	1.22	4.2
NGC 2023/2024	2	104	11.12	11.12	0.16	103.10	0.42	0.42	0.80	8.7
NGC 2023/2024	3	15	3.00	2.71	0.19	9.36	0.39	0.43	0.27	20.0
NGC 2023/2024	4	11	0.87	0.87	0.08	2.34	0.15	0.15	0.24	0.0
NGC 2068/2071	1	89	46.39	2.36	0.35	109.96	0.59	0.62	0.71	12.4
NGC 2068/2071	2	30	7.71	1.94	0.29	31.93	0.15	0.06	0.34	26.7
NGC 2068/2071	3	66	6.70	6.22	0.19	67.22	0.42	0.47	0.58	15.2
NGC 2068/2071	4	23	2.73	2.73	0.17	12.21	0.48	0.48	0.34	4.3
NGC 2068/2071	5	20	1.24	1.24	0.26	8.82	0.27	0.27	0.28	15.0
NGC 2068/2071	6	15	0.64	0.64	0.10	1.97	0.44	0.44	0.44	0.0

Notes.
[a] Total number of cluster members.
[b] Maximum core flux, maximum starless core flux, median core flux of individual cluster members, and the total flux of all cores in the cluster. Under the assumption of a constant dust temperature and opacity, the ratio of maximum to median flux is equal to the ratio in the mass of the most massive core to the median mass.
[c] Offset from the cluster's center of the highest flux core and the highest flux starless core, and the median offset of all cores.
[d] The fraction of cluster members which are associated with a *Spitzer* or *Herschel* YSO.

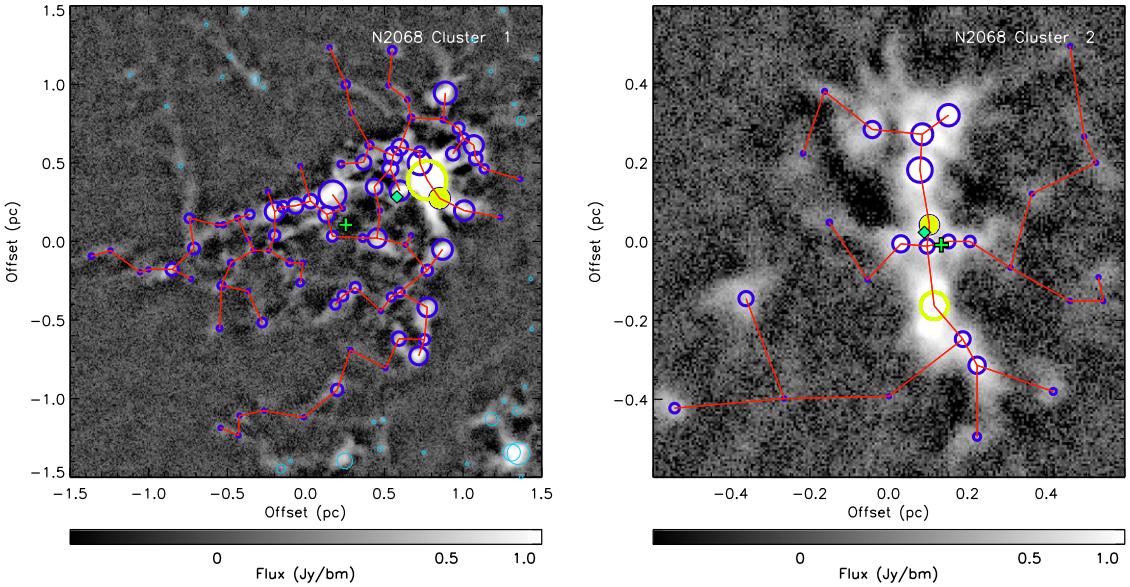

Figure 4. Zoomed-in view of the largest two MST-based clusters identified in NGC 2068/2071. The circles indicate the relative locations of dense cores, with the circle size scaling with the total core flux. Thicker dark blue circles denote cluster members, while thin light blue circles indicate non-members in the vicinity. The yellow open and filled circles indicate the locations of the highest flux cluster member and highest flux starless core cluster member respectively. The red lines indicate the MST structure after branches longer than L_{crit} have been removed. The green plus sign indicates the cluster center (median position), while the filled turquoise diamond indicates the flux weighted mean core position.

randomly located most massive members tend to have equal incidences of offset ratios above and below one. In Figure 5, we show the distribution of offset ratios found for dense core clusters in Orion B, as well as their "mass ratios". Here, we define "mass ratio" as the ratio between the flux of the highest flux cluster member and the median cluster member flux. For a constant conversion factor between flux and mass (see the discussion below), this ratio in fluxes is identical to that of the masses. The mass ratio is a very rough proxy for the degree to which the most massive cluster member dominates the system gravitationally, namely ratios near one indicate that all cluster members have similar fluxes (and hence masses), while high ratios indicate a diversity in fluxes and masses. We note that we do not perform any quantitative analysis using the mass ratio and use it in Figure 5 purely for illustrative purposes. Appendix B discusses in detail the sources of potential bias in our measurement of the offset ratio, and shows that if any bias is present, it serves to slightly increase the offset ratios measured here.

Figure 5 also shows the mass and offset ratios for clusters of dense cores identified in Orion A by J. Lane et al. (2016, in preparation). There, they use a different core-identification technique, but the same procedure for identifying clusters of cores and measuring offset ratios. In both Orion B and Orion A, it is clear that the majority of clusters have centrally located highest flux members.

We also compared the offset ratio distributions to those expected from random core locations. We created 10,000

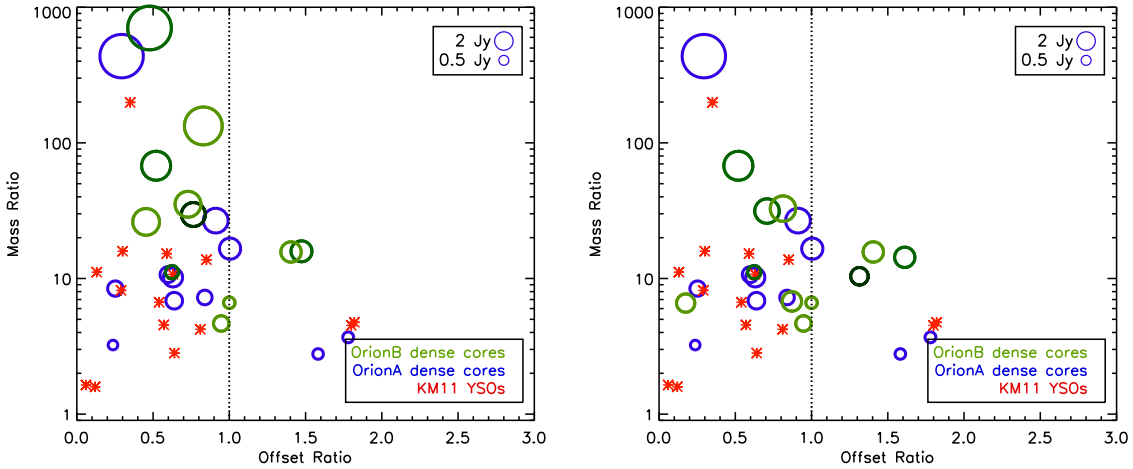

Figure 5. Comparison of mass and offset ratios for the dense core clusters in Orion B (green circles). The size of the circles scale with the total flux of the most massive dense core in the cluster, and the circle shading indicates the region (L1622, NGC 2023/2024, and NGC 2068/2071 correspond to darker through lighter shades of green). For comparison, the blue circles indicate dense core clusters measured using the same technique by J. Lane et al. (2016, in preparation), and the red asterisks show the YSO clusters analyzed in KM11. The left panel shows the results considering the full population of dense cores in each cluster, while the right panel shows the results for the highest flux/most massive *starless* dense core in each cluster.

synthetic clusters with either a uniform 2D (circular) or uniform 3D (spherical) distribution, randomly assigning one of the cluster members to be the most massive one. From these clusters, we calculated the nominal cluster centres and offset ratios using the same procedure as for the observations. We tried this test for clusters with 15, 25, and 50 members. For the Orion B clusters alone, a two-sided Kolmogorov–Smirnov test (Conover 1999) gives a probability between 11% and 17% of the observed offset ratios being drawn from any of the random distributions we tested. Combining the offset ratios for both Orion A and B clusters, the probability of being a random distribution drops to between 3% and 4%. The decreasing probability is primarily attributable to the increased sample size, as the fraction of clusters with offset ratios above one is similar in both samples (much less than 0.5), whereas the random samples all have fractions of clusters with offset ratios above 1 which are very close to 0.5. A direct comparison of the Orion B and A offset ratios with a two-sided KS test yields a probability of 74% of similarity, which is not statistically significant.

The offset ratios measured for the dense core clusters in Orion B and Orion A also bear a striking resemblance to the offset ratios KM11 measured for small, nearby, YSO clusters (red asterisks on Figure 5). A direct comparison between the offset ratios in KM11 and those of Orion B (and Orion A), however, requires two assumptions. First, the flux-ranking is the same as the mass-ranking of the dense cores, and, second, the most massive protostar tends to form out of the most massive core.

Regarding the first assumption, we know that it will not always hold, as hotter dense cores will appear brighter for the same intrinsic mass. Protostellar cores in particular can be expected to be hotter. Indeed, several protostellar cores in Orion B are known to have temperatures of order 50 K, which would imply masses about 3.3 times smaller than those obtained for a 20 K temperature (see discussion in K16). We therefore re-ran our analysis of the Orion B clusters selecting the highest flux *starless* dense core in each cluster, to account roughly for the potential bias introduced in flux measurements in the protostellar cores. The highest flux starless core in each cluster is also noted in Figures 4, 10, and 11. In some clusters, the highest flux core is actually starless, so our derived offset ratio is unchanged. In the remaining clusters, while the individual offset ratio measures change, the overall distribution of values remains fairly similar, as is illustrated in the right panel of Figure 5. This test indicates that our measurement of typically small offset ratios is true for both the highest flux core and the most massive core.

A two-sided KS test comparing the Orion B and A dense core cluster offset ratios with the KM11 YSO cluster offset ratios yields a probability of 24% of similarity, also inconclusive due to the small sample sizes. The fraction of offset ratios greater than one is somewhat smaller for the YSO cluster sample (15%) than for the combined dense core sample (22%). If the most massive YSO is formed from the most massive core, this difference in offset ratios could imply evolution in the position of the most massive cluster object between the dense core and YSO stage. Evans et al. (2009) estimate a lifetime of 0.54–0.7 Myr for the Class 0 plus I phases of YSOs (while Heiderman & Evans 2015, give an updated value of 0.54 Myr), which, for cluster velocity dispersions of 0.5–0.9 km s^{-1} (Foster et al. 2015), would correspond to a maximum motion of 0.3–0.6 pc. A second estimate of the typical velocity dispersion within clusters can be obtained through a combination of the YSO-to-core velocity dispersion, estimated to be about 0.1–0.2 km s^{-1} based on the offsets of embedded YSOs from the parent dense core (e.g., Jørgensen et al. 2007, 2008; Mairs et al. 2016, submitted) with the core-to-core velocity dispersion within a clustered environment, estimated to be several times larger. For example, the line of sight velocity dispersion between cores in clustered environments is 0.3–0.8 km s^{-1} in Perseus (Kirk et al. 2007). The total YSO-to-YSO velocity dispersion using this second technique is therefore similar to the Foster et al. (2015) result. Over the typical lifetime of an embedded YSO, the amount of motion possible is large enough to have a significant impact on the offset ratios of the smaller clusters in our sample. It is also possible, however, that Orion B and A represent a different cluster-forming environment than the KM11 sample (e.g., KM11's sample includes Taurus YSOs which typically have lower source-source surface densities than found in Orion B–see Section 4), so that the two samples cannot be thought of as direct correspondents at different ages. Further complicating the direct evolutionary picture, as noted in Section 2, is the fact that different cores may exhibit differing

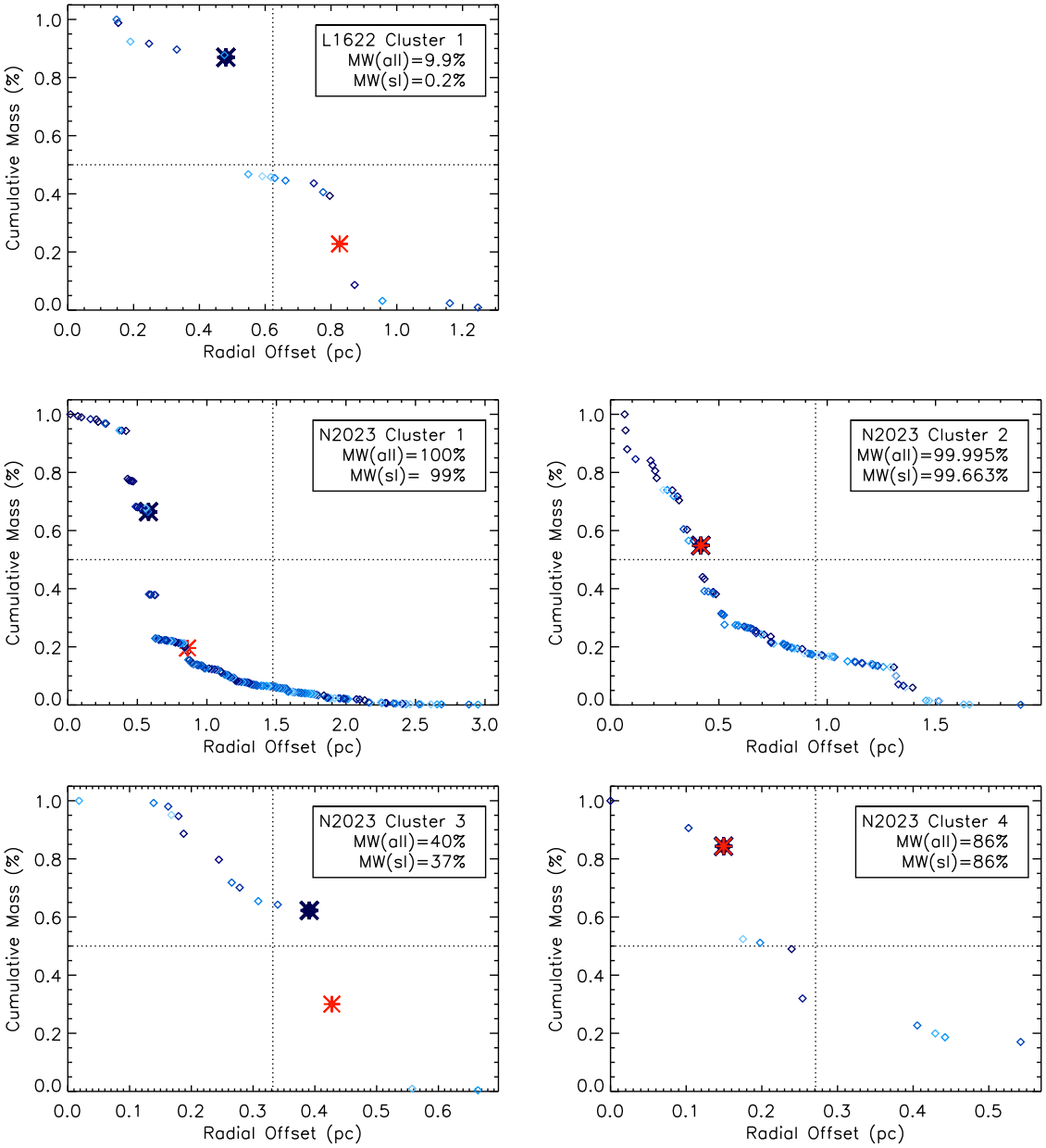

Figure 6. Cumulative mass of sources at a given offset or larger from their MST-based cluster center. The flux/mass rankings of the cores are indicated by the shading with darker indicating higher flux, the large dark blue asterisk indicating the highest flux member of each cluster, while the bright red asterisk denotes the highest flux starless core within each cluster. The horizontal dotted line indicates a cumulative mass fraction of 50%, while the vertical dotted line indicates half of the maximum offset. The Mann–Whitney probability that the inner half of the dense cores have typically higher fluxes than the outer half of cores is given in the upper right corner of each panel, for both the entire cluster population ("all") as well as only the starless cores ("sl"). This figure shows the clusters in L1622 (top row) and NGC 2023/2024 (middle and bottom rows).

amounts of fragmentation, and the least massive cores might dissipate without forming any protostars.

3.2. Beyond the Offset Ratio

In addition to measuring the offset ratio as a proxy for mass segregation, we briefly take a more qualitative look at the general tendency of higher flux cores to be located closer to cluster centres. Figures 6 and 7 show the cumulative distributions of dense core masses as a function of offset from the cluster centre for dense core clusters in Orion B. Visually, many of the clusters appear to have a higher fraction of high flux cores closer to the cluster centre. We test this hypothesis by running a Mann–Whitney (MW), or Wilcoxon, test (Conover 1999), also used by Kirk & Myers (2012) on the dense core fluxes in the inner and outer halves of the clusters. The MW test compares the rank order of values within the two sub-samples to calculate the probability that one sub-sample has typically larger or smaller values than the other. The probability that the inner half of the dense cores have higher fluxes than the outer half are reported in the legend of each panel in Figures 6 and 7. We ran this test for both the full cluster population, and examining only the starless cores. Indeed, several of the clusters do show strong signs of having more massive cores closer to the centre. For example, NGC 2023/2024 clusters 1 and 2 and NGC 2068/2071 clusters 1, 2, and 3 all have probabilities above 95% of higher flux

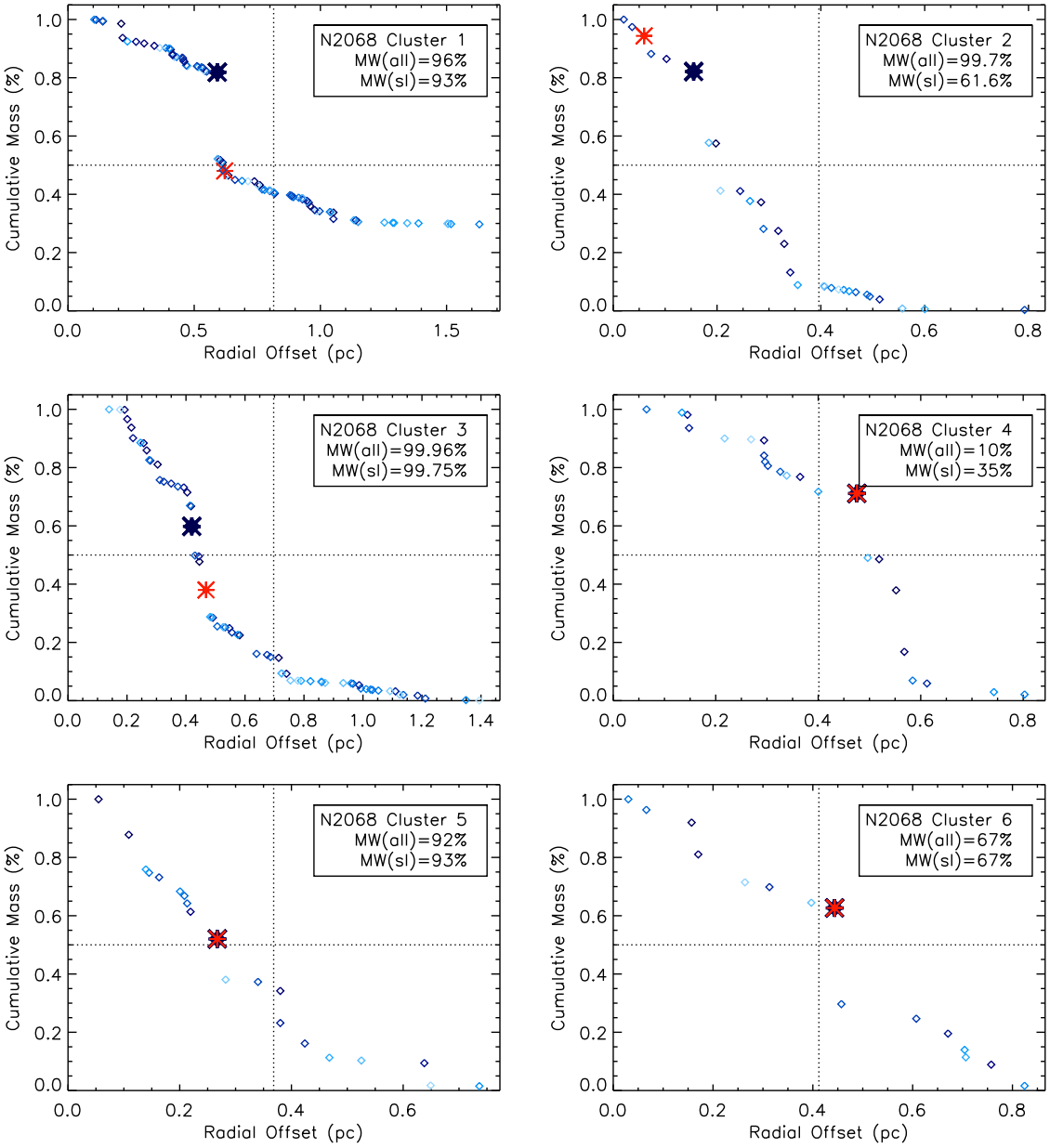

Figure 7. Cumulative mass fraction of sources at a given offset or larger from their MST-based cluster center, for clusters identified in NGC 2068/2071, showing the relative flux/mass rankings of the cores. See Figure 6 for the plotting conventions used.

members in the inner half (although NGC 2068/2071 cluster 2 has a lower probability for only the starless core population), while several other clusters have somewhat high probabilities. L1622 has a notably low probability, indicating a tendency for higher fluxes of dense cores in the *outer* half, i.e., a probability of 0.2% that the inner starless cores have higher fluxes and correspondingly a 99.8% probability that the outer cores have higher flux. Cluster 4 in NGC 2068/2071 also has a low, but less statistically significant probability.

4. LOCAL SURFACE DENSITIES

A second complementary method for measuring mass segregation that also works well in regions with substructure is presented in Maschberger & Clarke (2011). Their method does not explicitly subdivide sources into clusters, like the MST technique, but instead uses the local surface density of sources to distinguish between cluster centres and outskirts. The local surface density of sources is estimated using the separation to the *N*th nearest neighbor,

$$\sigma_N = \frac{N}{\pi r_N^2}, \quad (1)$$

where r_N is the distance to the *N*th nearest neighbor. This estimate has a fractional uncertainty of $N^{-0.5}$ (Casertano & Hut 1985; Gutermuth et al. 2009).[17] Maschberger & Clarke

[17] We note that these formulae are written with *N*-1 in the references listed, because there, the *N*th nearest neighbor is calculated at every location in an image, not only for a pre-defined list of sources. In the former case, finding the *N*th nearest neighbor at the position of a source would include the source itself, i.e., the second nearest neighbor would be the closest source to the one in question. Since in most other contexts, the *N*th nearest neighbor doesn't count the source itself for *N*, we adopt this terminology here. In the previous example, the source would be called the first nearest neighbor.

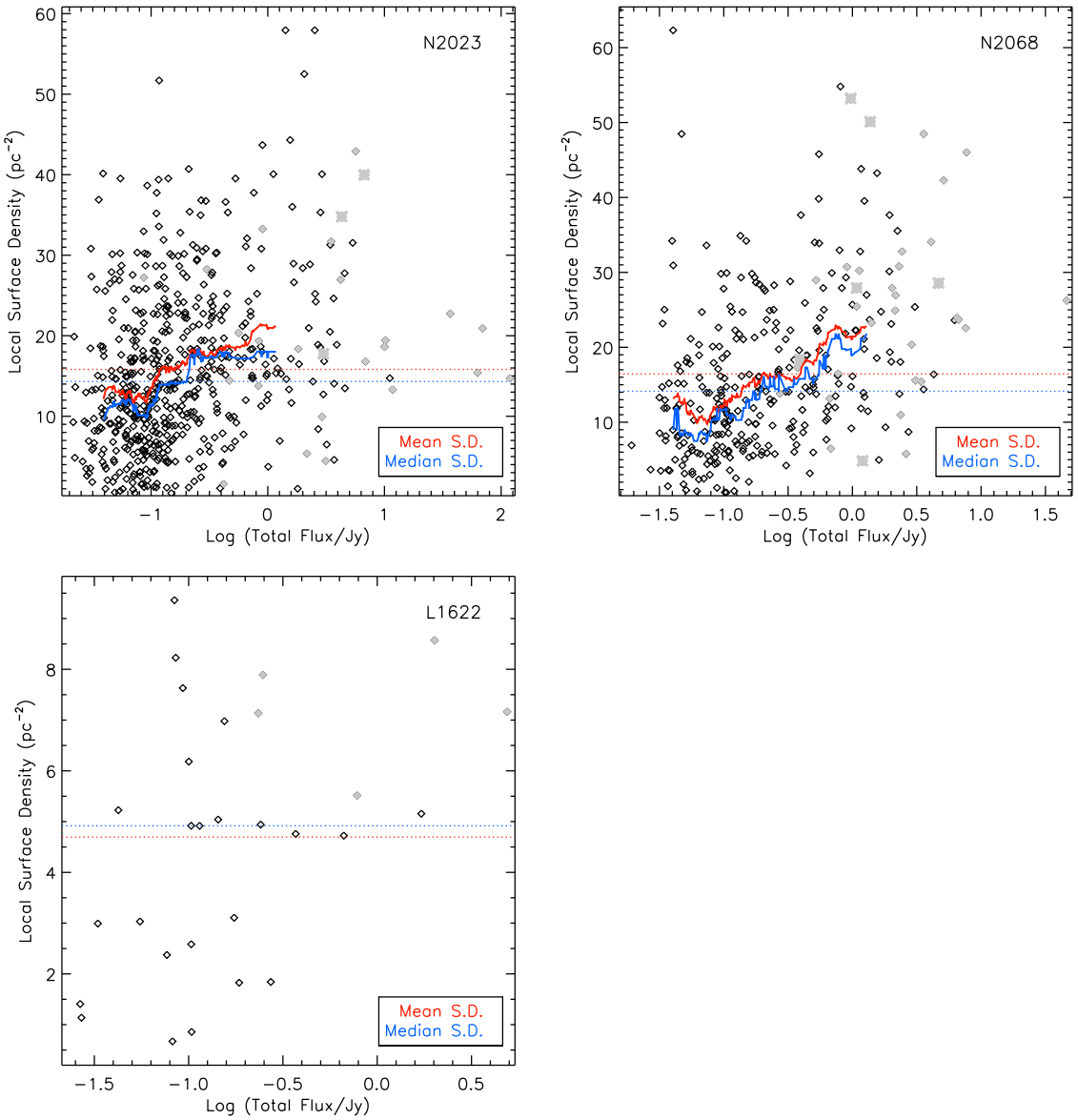

Figure 8. Comparison of the local surface densities of cores and their total fluxes. The top row shows NGC 2023/2024 and NGC 2068/2071 (left and right), while the bottom row shows L1622. In each plot, the five nearest neighbors were used to determine each core's local surface density (see text for details). Protostellar cores are denoted as the gray solid diamonds (using the Megeath et al. 2012, *Spitzer* catalog) and gray asterisks (using the Stutz et al. 2013, *Herschel* catalog). The solid red and blue lines in the top row show co-moving mean and median surface density values for the starless cores; a co-moving window of 40 starless cores was used for NGC 2023/2024 while a window of 20 starless cores was used for NGC 2068/2071. The dotted red and blue lines show the global mean and median surface density. In L1622, there were insufficient cores to calculate co-moving window values.

(2011) used $N = 6$ for their analysis and we tried both $N = 5$ and $N = 10$, and find similar results. Only the $N = 5$ results are shown here.

Once a source's local surface density has been estimated, mass segregation, if present, should manifest itself as a positive trend between source mass and local surface density. In all three maps of Orion B, we find that more massive (higher total flux) dense cores tend to inhabit areas with higher core surface densities. Figure 8 shows the dense core surface densities and total fluxes for each of the three regions. Protostellar cores, which may have higher fluxes due to their elevated temperatures, are shown in light gray. Although the correlation is not tight, it is clear that all three regions have a relative absence of cores in the top left (high surface density, low total flux) and bottom right (low surface density, high total flux) corners. Following Maschberger & Clarke (2011), we calculated the co-moving mean and median of the core surface densities as a function of total flux. We used a window full width of 40 starless cores in NGC 2023/2024 and 20 starless cores in NGC 2068/2071. The results are shown as the red and blue solid lines in Figure 8 and clearly highlight the trend for higher surface densities around higher flux cores. L1622, however, has too few cores for the co-moving mean and median analysis to be useful. In NGC 2023/2024 and NGC 2068/2071, the overall trend is unchanged with the window width adopted—we used the largest width feasible in order to best highlight the overall trend while decreasing random variations. Independent of the co-moving windows, we also used a two-sided KS test to see whether or not the apparent trends were significant. In each region, we split the cores into lower and higher flux subsets for both the full sample of dense

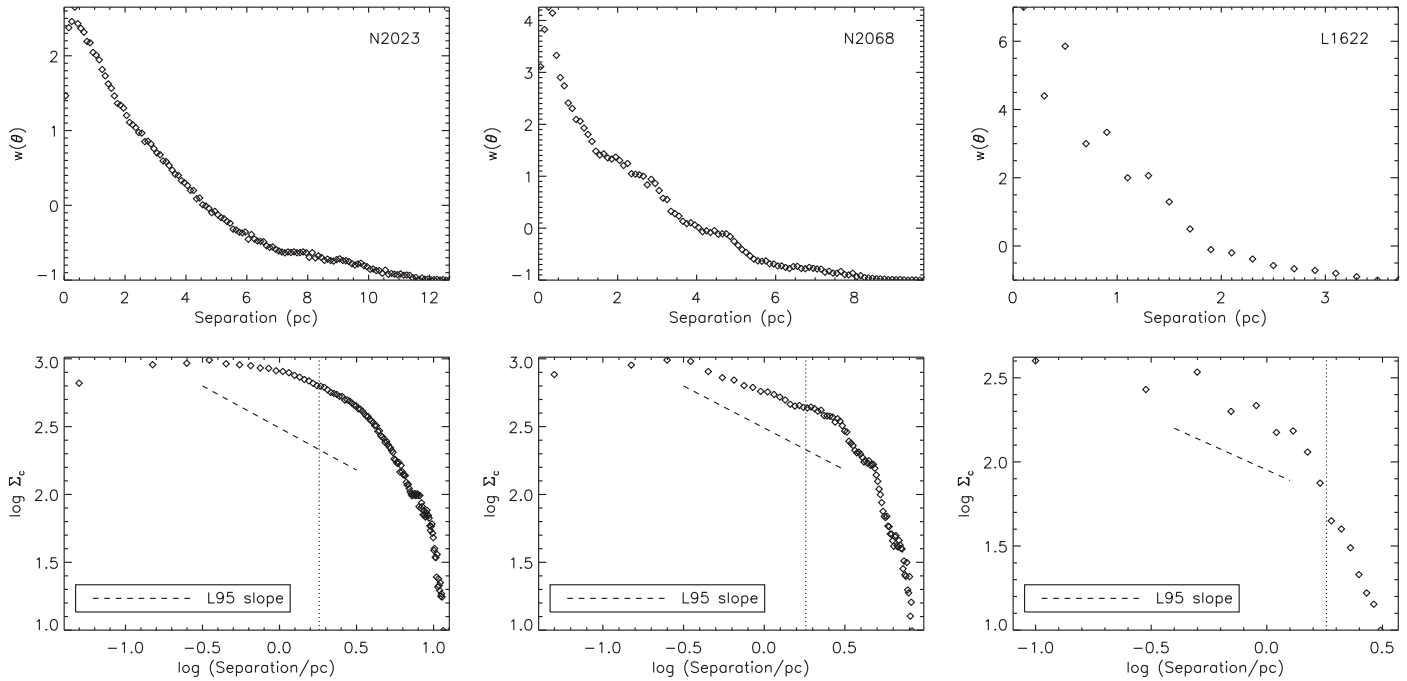

Figure 9. Two-point correlation function (top row) and surface density of companions (bottom row) for NGC 2023/2024 (left), NGC 2068/2071 (middle), and L1622 (right). The top panel is shown with a linear scaling to better illustrate substructure in NGC 2068/2071 while the bottom panel is plotted in the traditional log–log scale. The dotted line in the bottom panels shows the slope Larson (1995) fit at larger separations to the distribution of YSOs in Taurus. Note that the smallest one or two separation bins are likely incomplete due to the finite size of dense cores. In addition, the larger scales may be incomplete above a separation of ∼15′ (1.8 pc) due to the finite area observed. This upper scale is indicated by the vertical dashed line in the bottom panels.

cores and only the starless dense cores, and calculated the probability that the corresponding two sets of surface densities were drawn from the same parent sample. The resulting probabilities confirm what was visually suggested in Figure 8, namely that NGC 2023/2024 and NGC 2068/2071 show strong signs of dense core mass segregation, with probabilities of less than 10^{-5} regardless of how the high and low flux samples are split and using either $N = 5$ or 10 for the surface density calculation. L1622 has suggestive hints of the same trend when the protostellar cores are included in the analysis, but again has too few cores for this result to be statistically significant on its own (probabilities larger than a few percent).

5. OTHER CLUSTERING PROPERTIES

Moving away from mass segregation measurements, we also characterize the general clustering properties of each region. One commonly used measure of such properties is the two-point correlation function or the closely related surface density of companions (e.g., Gomez et al. 1993; Larson 1995; Simon 1997). The two-point correlation function, w, is defined as

$$w(\theta) = N_p(\theta)/N_r(\theta) - 1 \quad (2)$$

where N_p is the number of pairs of sources at a given angular separation, θ and N_r is the mean number of pairs of a random set of sources distributed over the same observed area (e.g., Gomez et al. 1993). The surface density of companions, $\Sigma(\theta)$, can be calculated as

$$\Sigma(\theta) = (N_{\rm tot}/A) \times (1 + w(\theta)) \quad (3)$$

where $N_{\rm tot}$ is the total number of sources and A the total area observed (Simon 1997).

We calculate $w(\theta)$ and $\Sigma(\theta)$ for each of the three regions in Orion B, and show the results in Figure 9. Two-point correlation functions effectively measure the degree to which sources are clustered together beyond what would be expected from a random distribution. Davidge (2012), for example, shows that a single cluster embedded in a lower density halo shows a change in w between the two regimes. Generally, two-point correlation functions are calculated for point sources, which our dense cores are not. Therefore, caution must be exercised at the smallest separation bins: clustering cannot be measured effectively on scales smaller that the size of a dense core. Since there is a range in core sizes, there is not a single cutoff value to apply to this distribution, but we estimate that the lowest two separation bins in Figure 9 may be affected. The lowest bin is certainly incomplete, due to the finite resolution of the observations. As with any two-point correlation function, the upper end of the distribution also becomes incomplete due to the finite areal coverage of the observations, although this effect is somewhat accounted for in w by comparison to a random distribution over an identical area. Within these two separation boundaries, we see that each of the three regions have a two-point correlation function that drops off steeply with increasing separation. All three have values of $w(\theta)$ above about 1 for size scales of ∼1.5 pc (∼12′), which roughly corresponds to the visual width of clusters within each region. In NGC 2023/2024 and L1622, $w(\theta)$ drops off fairly regularly with increasing separation, whereas NGC 2068/2071 shows several distinct bumps in the distribution. A visual inspection of the NGC 2068/2071 two-point correlation function indicates that the bumps correspond to typical size scales between clusters in the region. For example, the bump at 2–3 pc separations indicates the projected distance between neighboring clusters, while the bump at 4–5 pc corresponds to more

distant pairings of clusters. Although the main clusters of cores appear to be regularly spaced on first glance, a careful examination reveals a variation in separations of at least 50%, suggesting that the cluster-cluster separation cannot be explained in terms of simple thermal fragmentation analogous to that suggested on a smaller scale by Teixeira et al. (2006) in NGC 2264. The clusters in NGC 2023/2024 are even less regularly spaced, explaining the smoothness in w for that region, while L1622 only includes one obvious cluster.

Larson (1995) analyzed the surface density of companions of YSOs, Σ, in Taurus, and found two distinct power-law relations, with a break at ~0.04 pc, and a slope above this of $\Sigma \propto \theta^{-0.62}$. Simon (1997) found a similar result in YSOs in Ophiuchus, with a slope of –0.5, and a shallower slope in the Trapezium of –0.2, but argues that the three distributions are consistent with a value of –0.5 given the uncertainties. Larson (1995) and Simon (1997) interpret a single power law distribution as corresponding to an underlying fractal dimension of the molecular cloud of about 1.5 (2 plus the slope). Our measurements of Σ are shown in the bottom panels of Figure 9. At face value, none of the three regions appear to be consistent with a single power law relationship. As mentioned earlier, however, it is important to consider the area observed properly. Individual observations used in our mosaic are well-sampled to a diameter of ~30′, and in all three regions, this is a reasonable approximation to the narrowest map dimension observed. The surface density of companions, therefore, may not be well measured for separations above half of this diameter, or 15′. The vertical lines in Figure 9 show this limiting separation. Much of the curvature seen in Σ becomes apparent only above the limiting separation, suggesting that where the data is most reliable, a single straight power law with a slope similar to Larson (1995) or Simon (1997) is a reasonable approximation. Reassuringly, Johnstone et al. (2001) found a similar slope in their analysis of SCUBA observations of part of the NGC 2068/2071 region, with their best fit of $w(\theta) \propto \theta^{-0.75}$. It will be interesting to make this measurement for the larger contiguously observed regions in the GBS, such as Orion A, to see whether or not a single power law is representative of dense core clustering at the largest scales.

Next, we measured the clustering Q parameter following Cartwright & Whitworth (2004) for each of the three regions observed. Q is calculated as $\bar{m}/\bar{s}$, where $\bar{m}$ is the mean MST branch length, normalized by the factor $\frac{N-1}{\sqrt{N \times A}}$, N is the number of cluster members, A is the area of the cluster, and $\bar{s}$ is the mean separation of sources, normalized by the cluster radius, $R_{\rm circ}$. Cartwright & Whitworth (2004) find that values of Q above 0.8 correspond to clusters described by a single large-scale density gradient, while values of Q below 0.8 correspond to sub-clustered (fractally distributed) sources. We calculate A as the area contained within the convex hull[18] of each cluster, and $R_{\rm circ}$ as the maximum separation between a source and the cluster centre (calculated as the mean of the convex hull positions) following Gutermuth et al. (2009). We find Q values of 1.18, 0.99, and 0.91 for L1622, NGC 2023/2024, and NGC 2068/2071, respectively. All three values of Q nominally indicate a lack of subclustering, which is puzzling for NGC 2023/2024 and NGC 2068/2071 where subclusters are clearly visible. It is reassuring, however, that L1622, with no obvious subclusters, has the largest value of Q. We first rule out two possibilities raised by Cartwright & Whitworth (2009a, 2009b) for unexpected values of Q. Namely, none of the regions show signs of "anti-clustering," as indicated by normalized mean separation of sources above 0.8, or are sufficiently elongated to require a correction to the observed Q, as required for axial ratios greater than 3 and $0.9 < Q < 1$. There are several reasons why the values of Q we measure are generally higher than expected. First, our observations of the NGC 2023/2024 and NGC 2068/2071 regions each cover multiple groupings of cores that are somewhat linearly spaced and not circularly distributed. This spatial distribution makes the measurements of quantities such as $R_{\rm circ}$ much more difficult to define and measure. We tried calculating $R_{\rm circ}$ as the maximum separation from the mean source position, as well as half of the maximum separation between all cores. The former definition of $R_{\rm circ}$ increases the estimated Q values (up to 13% higher), while the latter decreases the estimated Q values (about 2% lower). While none of these variations place the value of Q measured for NGC 2023/2024 and NGC 2068/2071 into the "subclustering" regime, they do highlight the fact that such non-circular core locations can make it difficult to measure Q accurately. A second possibility is that the application of a point-source measure like Q to dense cores either introduces a larger source of error or changes the value at which subclusters versus a single radial density gradient are indicated. Testing using synthetic distributions of clusters of cores (beyond the scope of this work) would be necessary to determine if and how Q should be re-calibrated for this application.

[18] A convex hull is a shape with the minimum area required to enclose a set of points under the condition that all neighboring boundary segments form >90° angles.

6. DISCUSSION

6.1. Clustering Measurement Methods

The existence of mass segregation in young stellar clusters, and whether it is attributable to a primordial distribution or dynamics, is an ongoing debate. Girichidis et al. (2012) point out that major challenges are the coupled problems of determining whether sub-clustering is present and how to define mass segregation itself. The local dynamical timescale for a sub-cluster can be significantly smaller than the global dynamical timescale, and therefore a region can become mass segregated in less than a global dynamical timescale due to stellar interactions within the sub-clusters (Allison et al. 2009a; Moeckel & Bonnell 2009; Maschberger & Clarke 2011; Girichidis et al. 2012). Tied to this issue is whether the mass segregation itself is measured locally or globally. For example, Kirk & Myers (2011) find that YSOs within Taurus are mass segregated by examining the relative location of the most massive YSO within each sub-cluster. At the same time, Parker et al. (2011) find that the entire Taurus complex is *inversely* mass segregated: the most massive YSOs are further apart from each other than typical YSOs are in the complex. Taurus has an unusual YSO spatial distribution, with largely separated sub-clusters (especially those harbouring the most massive YSOs in the complex), and very few YSOs found anywhere near its geometric centre. In the case of Taurus, the very dispersed distribution of YSOs coupled with the near-thermal velocity dispersion of material (e.g., Seo et al. 2015) make it clear that the Kirk & Myers (2011) and Parker et al. (2011) analyses are tracing very different scales of processes. The age of the YSOs in Taurus is much less than the region crossing-time, and so sub-clusters across Taurus have not had time to interact. In

other regions, the scale appropriate for measuring a cluster's mass segregation may be less obvious.

Parker & Goodwin (2015) recently compared three different mass segregation analysis techniques: the Allison et al. (2009b) $\lambda_{\rm MST}$ technique (used in Parker et al. 2011, discussed above), the Maschberger & Clarke (2011) M–Σ method discussed in Section 4, and the Kirk & Myers (2011) MST-group analysis discussed in Section 3. The $\lambda_{\rm MST}$ method effectively considers a population of sources as a single cluster, and determines whether or not the more massive sources are located closer together than a comparable random sample of sources. The M–Σ method allows for the possibility of a monolithic cluster or sub-clustering, and measures whether or not more massive sources tend to be located in regions of higher than average surface density of sources. The MST-group analysis tends to assume that a system is made up of distinct sub-clusters, and examines whether or not in each one the most massive source is more centrally located than is typical.

In their study, Parker & Goodwin (2015) create a fractal YSO distribution with several different assignments of mass to the YSOs, and test the ability of each of the three techniques to measure correctly the presence or absence of mass segregation. As expected, the $\lambda_{\rm MST}$ method fares best when the mass segregation is set up in a way that matches how the method detects it e.g., closely located massive stars. Also, the M–Σ method fares best when the most massive stars are inserted in regions of high local surface density. Parker & Goodwin (2015) did not include a third test tuned to the strengths of the MST-group method, i.e., centrally located most massive members in sub-clusters, so it is not surprising that this method fared the worst of the three in their comparisons. Parker & Goodwin (2015) correctly point out that the MST-group method tends not to measure mass segregation for all of the N most massive sources (specifically ten in their synthetic distributions), since larger sub-clusters tend to contain multiple more-massive sources while smaller sub-clusters may only contain relatively low mass sources. Instead, the MST-group method makes measurements based on the relative masses of each sub-cluster. This situation highlights the importance of clarity in defining what is meant by mass segregation and how it is being measured.

Another point alluded to by Parker & Goodwin (2015) is that the MST-group method can only produce reliable results if the sub-clusters identified are distinct physical entities. While subclustering can be difficult to determine in practice, one important component lacking in the Parker & Goodwin (2015) analysis is a careful consideration of uncertainties in sub-cluster membership based on the MST-based criterion for group definition. If sub-cluster membership is highly uncertain (due to, say, uncertainties in $L_{\rm crit}$), very different mass segregation estimates result, then the MST-group results should be treated as being questionable. This uncertainty underlines the importance of ensuring the sub-clusters are well-defined (preferably also visually distinct) before embarking on any further analysis. Conversely, when there are obviously distinct sub-clusters, the $\lambda_{\rm MST}$ method (unless applied separately to each sub-cluster) is then better at tracing bulk properties of the region imprinted at formation and not the present mass segregation in each sub-cluster. Where distinct sub-clusters are present, as in the Taurus example discussed above, the typical separation between the most massive members measured by the $\lambda_{\rm MST}$ technique is more influenced by the spacing between sub-clusters harbouring massive members than it is to the local mass segregation.

In NGC 2023/2024 and NGC 2068/2071, there are very visually distinct groupings of dense cores separated by several parsecs. HARP CO(3-2) observations show a typical linewidth of $C^{18}O/^{13}CO$ of 1–3 km s^{-1} across the two regions (Buckle et al. 2010). This dispersion is likely to be higher than that of the denser gas, and therefore can be used to provide a lower limit to the interaction timescale between the groups of roughly 1 Myr, i.e., the time to travel several pc at several km s^{-1}. Dense cores detectable at submillimeter wavelengths have an estimated lifetime several times smaller than this, i.e., several tenths of a Myr (e.g., Kirk et al. 2005; Hatchell et al. 2007; Enoch et al. 2008), although recent *Herschel* results in Aquila suggest that the full population of dense cores there may have a lifetime closer to 1 Myr, while higher density cores ($n_{\rm H2} > 10^5$ cm^{-3}) have lifetimes of 0.4 Myr or less (Könyves et al. 2015). While these estimates are necessarily approximate, they do suggest that there has been insufficient time for many interactions between the clusters we identify, and hence that it is sensible to characterize mass segregation on the scale of these clusters, rather than the region as a whole. The fact that our error analysis (see Appendix B) shows our results are robust to reasonable variations in the cluster definitions for the MST-group analysis, and that a similar conclusion is reached using the independent M–Σ method supports our findings of mass segregation within these dense core clusters.

6.2. Implications

Dense cores are in a particularly interesting regime to measure clustering properties. On the one hand, they provide the initial conditions for the formation of (proto)stellar clusters and should be taken into account in cluster modeling. On the other hand, dense cores are themselves the product of the history of substructure formation within the molecular cloud, and continue to evolve through processes including mass accretion and gravitational collapse, and their present-day properties may provide some insight into these. To the best of our knowledge, predictions of the clustering properties of dense cores have not yet been made either theoretically or using numerical simulations. We therefore suggest that our observations be included as a benchmark test in future work. It will also be helpful to expand the measurement of dense core clustering properties to additional systems where the local environment (or even the age of the system) may have influenced the present-day appearance of dense core clusters in a different way than in Orion.

The study of clustering properties in stellar and protostellar systems has been well studied both theoretically and observationally. Numerical simulations have varied predictions on whether or not there is primordial mass segregation in clusters. Some simulations find mass segregation of stars/sink cells in clusters from very early times (e.g., Maschberger & Clarke 2011; Girichidis et al. 2012; Kirk et al. 2014; Myers et al. 2014). Other simulators find no evidence of mass segregation (e.g., Parker et al. 2014), while Parker et al. (2015) find that evidence for or against mass segregation depends on the method used to measure it.

Observations of mass segregation are somewhat divided, although it appears that the majority of studies do indicate some degree of mass segregation is common. Young stellar clusters tend to show signs of present-day mass segregation, which,

given the approximate age of the systems, is often interpreted as implying that the segregation is at least partially primordial (e.g., Carpenter et al. 1997; Bonnell & Davies 1998; Hillenbrand & Hartmann 1998; Gouliermis et al. 2004; Stolte et al. 2006; Gennaro et al. 2011; Kirk & Myers 2011; Davidge 2015). Note, however, that in more crowded systems, there are several observational biases which need to be carefully considered to measure true mass segregation (Ascenso et al. 2009). Several recent studies, however, do not find evidence of primordial (and in some cases, even present-day) mass segregation (e.g., Allison et al. 2009a, 2010; Parker et al. 2012; Wright et al. 2014).

Looking at even younger systems, observations appear to favor mass segregation. Megeath et al. (2005) and Hunter et al. (2006) find small, tight groupings of very young, high-mass, protostars in W3 IRS-5 and NGC 6334, respectively, which are surrounded by a larger cluster of low- and intermediate-mass stars (see, however, Hunter et al. 2014, for an example of a young protocluster system where the most massive member is not centrally located). Similarly, Kryukova et al. (2012) and Elmegreen et al. (2014) examine young protostars (primarily or entirely Class I, respectively), and find that the highest luminosity protostars tend to be found in regions of higher source surface density. We note that the Kryukova et al. (2012) protostar sample includes Orion A and B along with several other nearby star-forming regions. Since high protostellar luminosity is caused by either high intrinsic source luminosity, implying a high-mass protostar is already present, or a high accretion rate, implying a high-mass protostar is likely forming, these observations also suggest that some mass segregation is imprinted at the start of the protostellar formation phase, as insufficient time has passed for there to be subsequently significant motions (Elmegreen et al. 2014). Furthermore, Elmegreen et al. (2014) finds evidence of "collaborative accretion," i.e., neighboring protostars tending to have similar luminosities, perhaps implying they all are accreting from a locally high density zone of material. Zhang et al. (2015) argue for a similar picture based on high-resolution observations of a high-mass star-forming infrared dark cloud. The cluster-forming gas is densest in the centre, which allows for the most massive stars to (start) form(ing) there first, while lower mass star formation can continue for longer in the lower-density outskirts (see also the discussion in Myers 2011, about star formation timescales as a function of final stellar mass).

Our observations that dense core clusters are somewhat mass segregated support the hypothesis that the centre of forming clusters provide a more favorable environment for the most massive protostars to form, with more dense gas available at the cluster centre for local accretion. We emphasize that this does not rely on a one-to-one mapping between dense core mass and final protostellar mass, rather merely that the most massive protostars form out of the most massive (and densest) dense cores. The picture of more massive protostars forming in a cluster centre due to the favorable conditions there is consistent with the competitive accretion scenario (e.g., Bonnell et al. 2004). That model, however, typically assumes initially equal mass protostellar seeds to track subsequent gas accretion, and it is unclear what the spatial distribution of dense cores would be in the model. Krumholz et al. (2007) argue that radiative effects, while often overlooked in simulations, can be of key importance to determine how much fragmentation occurs.

The one aspect that our current study cannot address is the effect of environment. Our results, coupled with those of dense cores in Orion A (J. Lane et al. 2016, in preparation) show that in the denser, more active star-forming environments of our local Gould Belt clouds, dense cores are mass segregated within their local clustered environments. The next step is to determine whether this same property holds true in sparser, more quiescent star-forming regions such as Taurus, which we are in an excellent position to examine with the full JCMT GBS dataset available.

7. CONCLUSION

We examined the clustering properties of the dense cores in the L1622, NGC 2023/2024, and NGC 2068/2071 regions of the Orion B molecular cloud. In particular, we focused on mass segregation under the assumption that generally cores with higher total fluxes will form the highest mass protostars. Using two complementary and independent methods, we find that the dense cores are mass (flux) segregated in Orion B. A MST analysis (Section 3) shows that visually apparent clusters tend to have a centrally located most massive member, and often a general tendency for more massive members being located closer to the cluster centre. A comparison of the core mass and local core–core surface density shows that more massive cores tend to be found in more highly clustered environments. If the most massive protostars tend to be born within more massive dense cores, our result implies that mass segregation in stellar clusters may in part be imprinted already in the dense gas from which they form. An analysis of dense cores in the nearby Orion A molecular cloud also finds similar results. If dense core mass segregation holds over a wider variety of star-forming environments, these data provide a new observational test for simulations and theories of clustered star formation. It would also imply that clustering of stars can only be understood by studying the causes of (dense) substructure in molecular clouds.

The authors thank the anonymous referee and Eric Feigelson for comments which improved the paper and the presentation of our results. H.K. thanks Jonathan Tan for a conversation which helped to inspire some of this analysis and Phil Myers for some helpful comments on a draft of this paper. The authors recognize and acknowledge the very significant cultural role and reverence that the summit of Maunakea has always had within the indigenous Hawaiian community. We are most fortunate to have the opportunity to conduct observations from this mountain. The JCMT has historically been operated by the Joint Astronomy Centre on behalf of the Science and Technology Facilities Council of the United Kingdom, the National Research Council of Canada and the Netherlands Organisation for Scientific Research. Additional funds for the construction of SCUBA-2 were provided by the Canada Foundation for Innovation. The authors thank the JCMT staff for their support of the GBS team in data collection and reduction efforts. The Starlink software (Currie et al. 2014) is supported by the East Asian Observatory. This research used the facilities of the Canadian Astronomy Data Centre operated by the National Research Council of Canada with the support of the Canadian Space Agency. Figures in this paper were creating using the NASA IDL astronomy library (Landsman et al. 1993) and the Coyote IDL library (http://www.idlcoyote.com/index.html).

Facility: JCMT (SCUBA-2).
Software: Starlink (Currie et al. 2014), IDL.

APPENDIX A
MST-BASED CLUSTERS

Here, we present a series of snapshots of all of the dense core clusters identified using the MST technique across the three regions. Figures 10 and 11 show the clusters in L1622 and NGC 2023/2024, and NGC 2068/2071, respectively.

APPENDIX B
MST AND OFFSET RATIO ANALYSIS UNCERTAINTIES

B.1. Cluster Definition Uncertainties

As discussed in Kuhn et al. (2014), one important test for any non-parametric cluster model (such as our MST analysis), is a thorough check on the effect of the variation in user-specified values on the results. While Figures 10 and 11 show that the clusters we identify are visually reasonable, here, we explicitly test the impact of varying the $L_{\rm crit}$ and N (the minimum number of cluster members) on our results.

For each of the three regions, we tested a range of $L_{\rm crit}$ values, corresponding to the intersection of linear fits to the cumulative branch length distribution somewhat beyond the range of good fits. We used this range to determine the maximal impact of different values of $L_{\rm crit}$ on the definition and membership of the clusters, and how this then changes the results of the offset ratio measurements. Since it has relatively few cores, L1622 has the poorest best fit to the cumulative branch length distribution, and the largest range of "okay" fits. In our tests of this region, we set the maximum $L_{\rm crit}$ to be sufficiently large to include *all* cores in the cluster. In all other cases (minimum $L_{\rm crit}$ for L1622 and both minimum and maximum $L_{\rm crit}$ for the other two regions), we find $L_{\rm crit}$ varies less than 18% from the best fit values.[19] Within this range of $L_{\rm crit}$ values, we find that the main properties of most identified clusters change very little. In NGC 2023/2024, clusters 3 and 4 remain identical under the full range of $L_{\rm crit}$ values, while clusters 1 and 2 are identical for smaller $L_{\rm crit}$ values, but become merged into a single entity for large values of $L_{\rm crit}$. In NGC 2068/2071, clusters 1, 2, 4, and 5 remain nearly identical for the full range of $L_{\rm crit}$ values, with the occasional loss or gain of members at their peripheries. NGC 2068/2071's cluster 3 and 6 are similar for larger values of $L_{\rm crit}$ but for smaller $L_{\rm crit}$, cluster 3 is split into two clusters, and cluster 6 no longer has a sufficient number of members (i.e., more than 10) to be classified as a bona fide cluster. Interestingly, even with these significant membership changes, the inner part of cluster 3 and its centre position stay remarkably similar. L1622, with its wider range of possible $L_{\rm crit}$ values, shows a greater variation in membership, ranging from the inclusion of all cores for the largest $L_{\rm crit}$, and only 9 cores in the "cluster" for the smallest $L_{\rm crit}$. Despite the changes in some clusters' appearances, however, the overall distribution of cluster offset ratios remains remarkably similar. Changes in cluster membership often tend to be somewhat symmetric, i.e., members being added or subtracted from multiple sides of the cluster with an increase or decrease in $L_{\rm crit}$. As such, the cluster center tends to change very little with variations in $L_{\rm crit}$. Similarly, the median offset tends to vary little if only a few large offsets are included or excluded from the calculation, and hence the offset ratio tends to be similar for small changes to the cluster membership. We demonstrate the relative invariance in the offset ratios we measure in Figure 12. Regardless of the $L_{\rm crit}$ applied, the majority of clusters have centrally located most massive members.

Furthermore, we test the effect of changing the minimum number of cluster members on our results. From our standard requirement of $N > 10$, we try $N > 15$ and $N > 5$. A higher value of N serves to reduce our existing cluster sample. As can already be seen in Table 1, only three of our clusters have $N < 20$, and these three clusters are eliminated from our sample with an $N > 15$ requirement. Figure 13 shows that with these smaller clusters removed, our overall results are qualitatively unchanged: most clusters still have offset ratios less than one, with only one of eight clusters in this restricted sample having an offset ratio above one. When we decrease the minimum number of members required to be classified as a cluster, new clusters are added to the analysis; setting $N > 5$ adds six new "clusters," three each in NGC 2023/2024 and NGC 2068/2071, as the right panel of Figure 13 shows. Of these six additions, one has an offset ratio below one, three have offset ratios of exactly one, and two have ratios greater than one. These small-N "clusters" clearly have less of a tendency for a centrally located most massive member than their higher-N bretheren, but this is understandable. With such a small number of members, some of the "clusters" may not be physically associated. Even if they are associated, the offset ratio is strongly sensitive to the location of the cluster center which becomes ill-determined in the small-N regime. The small "clusters" identified also have a tendency to contain only very low mass members ($<$0.2 Jy for the NGC 2023/2024 "clusters") and the most massive member is often not very distinct (four of the six small "clusters" have most massive members which are less than three times the median mass). All of these factors lead us to expect to see less of a trend in the offset ratio for these very small-N clusters and do not take away support from our main findings.

B.2. Core Definitions and Resolution

Beyond the definition of each cluster, another source of uncertainty in our analysis of offset ratios is our definition of core boundaries and therefore their total fluxes. There are two potential issues which could influence which core we identify as having the highest flux, and therefore change the offset ratio measured. The first issue is substructure on scales smaller than the SCUBA-2 850 μm beam. Namely, depending on how the cores we identify fragment at smaller scales, we might identify a different highest flux core if using higher resolution observations. We test this possibility by examining the SCUBA-2 450 μm map, whose effective beamsize is nearly twice as small as the 850 μm map, and search for signs of fragmentation in cores near the cluster centers. Indeed, in the largest, highest density, clusters in NGC 2023/2024 and NGC 2068/2071 (cluster 1 in NGC 2023/2024 and clusters 1 and 2 in NGC 2068/2071), we see that the core flagged as the highest flux core shows signs of fragmentation. A careful examination of these fragmented cores shows one of two behaviors: (1) part of the highest flux core will likely still be the highest flux core even if the fragmentation is accounted for,

[19] The range of acceptable $L_{\rm crit}$ values for each region is as follows: 0.35–1.7 pc in L1622, 0.26–0.30 pc in NGC 2023/2024, and 0.23–0.29 pc in NGC 2068/2071.

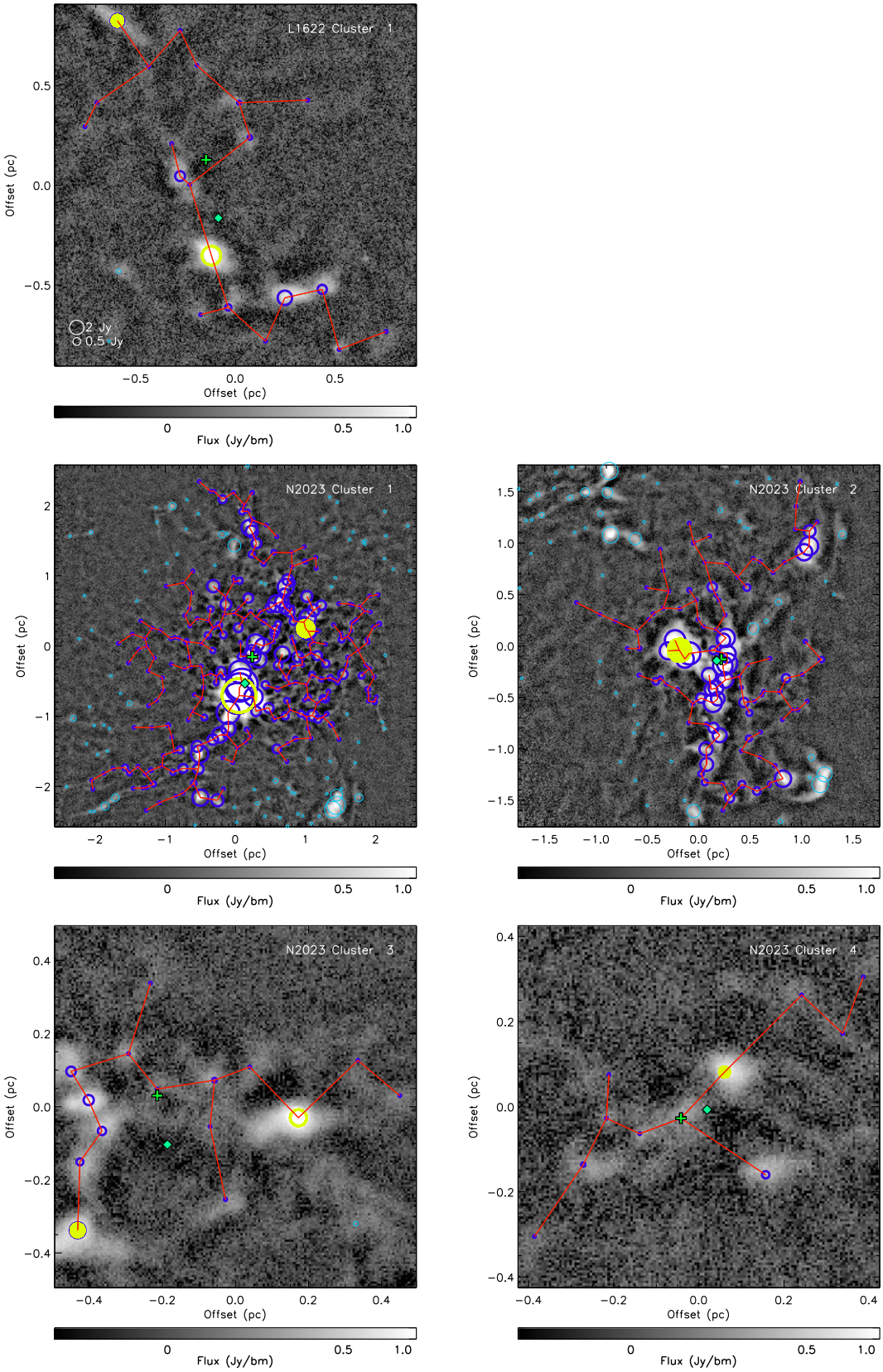

Figure 10. Dense core clusters identified in L1622 (top left panel) and NGC 2023/2024 (remaining panels) using MSTs. The background grayscale images show the SCUBA-2 850 μm map. The thick blue circles denote the positions of dense cores which are members of that cluster, while the thin teal circles denote non-cluster members. The size of the circle scales with the total flux (see legend in top left panel). The empty and filled yellow circles show the highest flux cluster member and starless core cluster member respectively. The red line shows the MST structure after branches larger than $L_{\rm crit}$ have been removed. The green plus symbol shows the cluster center, calculated as the median position of cluster members. The turquoise diamond symbol shows the flux-weighted mean core position.

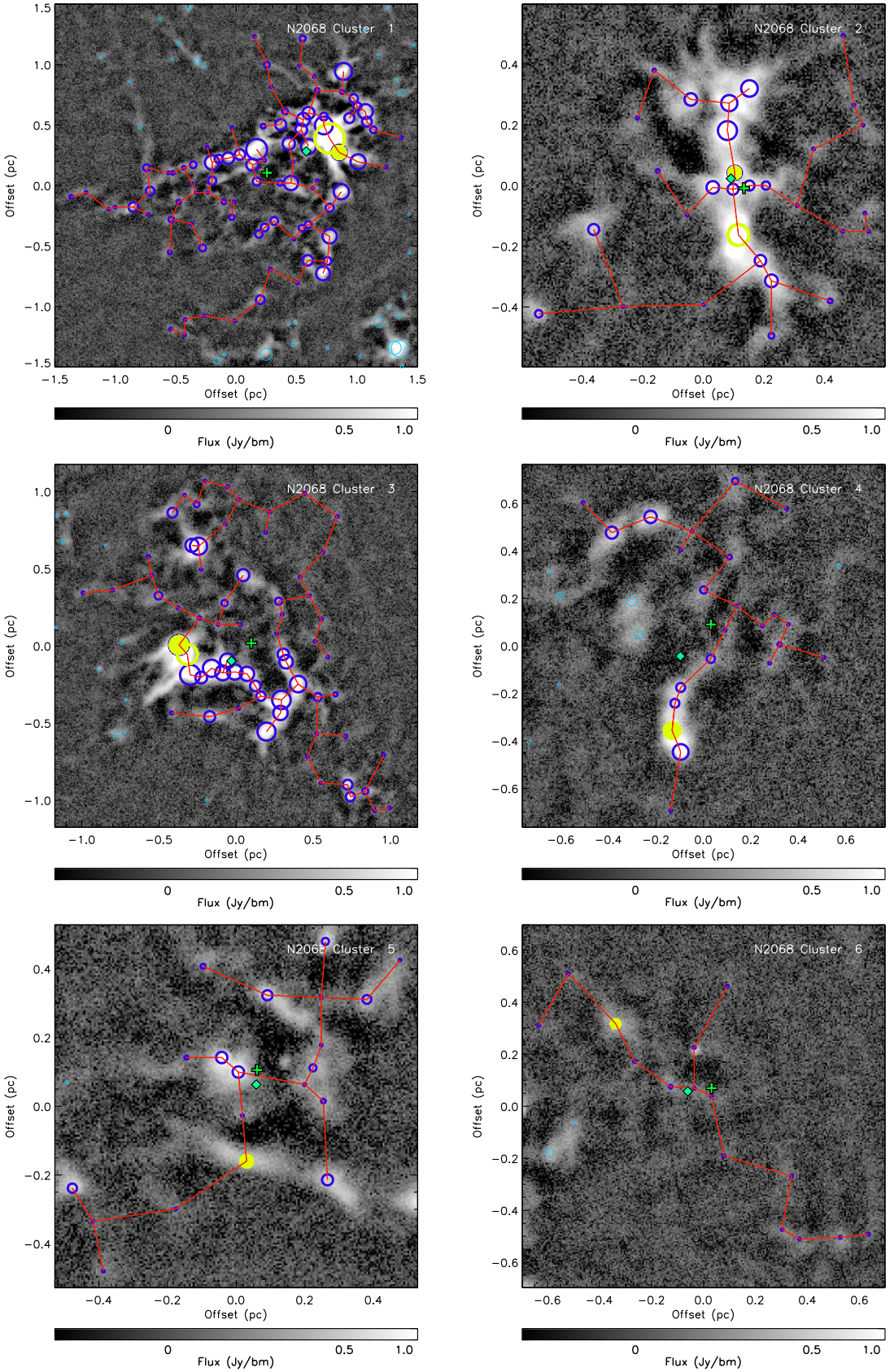

Figure 11. Dense core clusters identified in NGC 2068/2071 using MSTs. See Figure 10 for the plotting conventions used.

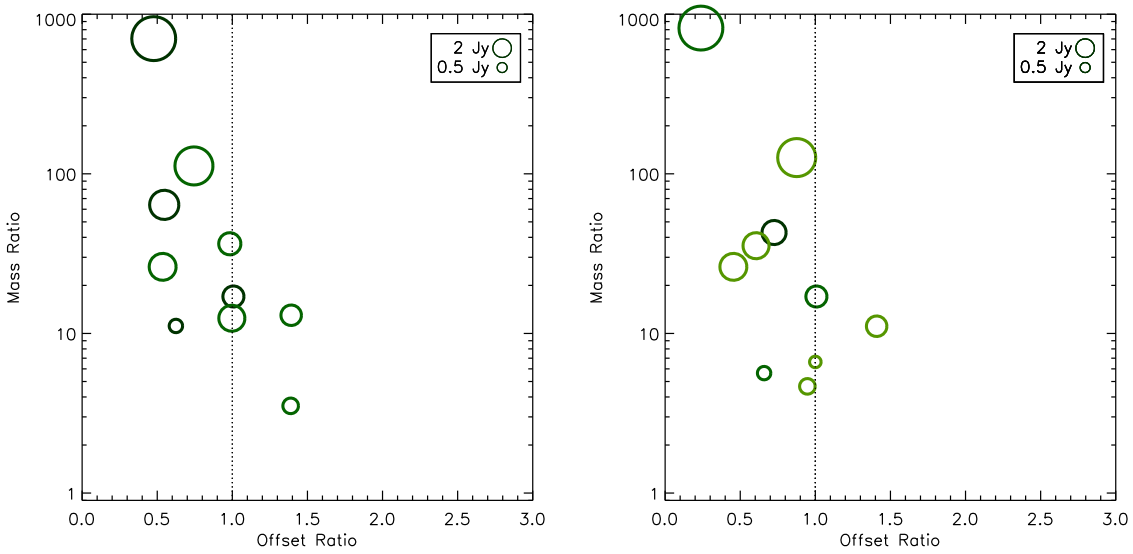

Figure 12. Comparison of the offset ratios measured when extreme values of $L_{\rm crit}$ are applied to the determination of cluster membership, using the full sample of dense cores. This can be compared to the left panel of Figure 5, where the green circles indicate the offset ratios for the originally determined clusters in Orion B. Left: the application of a small value of $L_{\rm crit}$. Right: the application of a large value of $L_{\rm crit}$. See Figure 5 for the plotting conventions used.

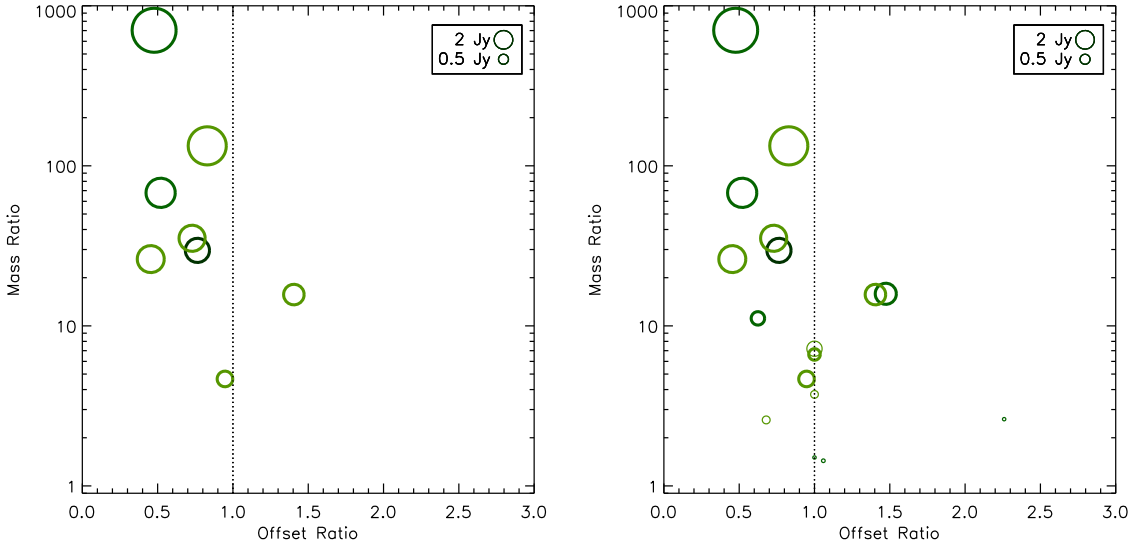

Figure 13. Comparison of the offset ratios measured when different values of N (minimum number of cluster members) are applied to the MST analysis using the full sample of dense cores. These figures can be compared to the left panel of Figure 5, where the green circles indicate the offset ratios for the originally determined clusters in Orion B. Left: $N > 15$ members. Right: $N > 5$ members, with members not satisfying the original $N > 10$ criterion shown with thinner circles. See Figure 5 for the plotting conventions used.

or (2) with fragmentation included, a different core would likely be flagged as the highest flux core, but this new core is at a comparable (or smaller) separation to the cluster center. Although it is possible that these results would change at even higher resolutions, it is reassuring that the results appear to be robust to at least modest improvements in resolution.

The second potential issue is the outer core boundary. Cores may have a high total flux due to being a bright compact source or due to having a large boundary encompassing a significant amount of more diffuse emission (or both). The fraction of material from a given core that will end up in the stars that form out of it is not clear, and could easily vary from core to core (and, similarly, the amount of material a protostar accretes from beyond the core may also vary). Nonetheless, there is a perhaps naive expectation that the "highest flux core" of interest in the offset ratio analysis is one that has a large amount of compact emission, rather than merely a large total flux due to a large areal extent of diffuse emission. We examine both the 850 and 450 μm emission maps to identify the sources of strong compact emission within each cluster, and whether or not these correspond to the cores flagged as the highest flux cores in our earlier analysis. In several cases (cluster 2 in NGC 2023/2024 and clusters 3, 4, 5, and 6 in NGC 2068/2071), the core with the largest amount of compact emission differs from the core with the highest total flux. In all but one of these cases (cluster 4 in NGC 2068/2071), the position of the brightest compact emission core lies *closer* to the cluster center than the core with the highest total flux, which would lower the offset ratios we measure.

In addition to these two tests, we note that Figures 6 and 7 show a general tendency for more massive cores to have smaller offsets, which also suggests that our choice of the most

massive core has a small influence on our results. We therefore conclude that our core definitions do not appear to bias artificially the offset ratio lower, due to either the resolution of the telescope or the precise core boundary adopted.

B.3. Cluster Centers

Finally, the offset ratio analysis depends on where the cluster center is located. Here, as in KM11, we adopt the median position as the cluster center. KM11 argue that using instead the center of mass as the cluster center has the potential to bias the center position toward the location of the most massive cluster member, and hence result in smaller offset ratio measurements. Our present analysis suggests a similar possibility. In Figures 10 and 11, the flux-weighted mean core position, i.e., the center of mass under the assumption of a constant conversion between flux and mass, is indicated in addition to median core position adopted as the cluster center. There is a clear tendency for the highest flux core to be located closer to the "center of mass" position than the median core position. Therefore, our offset ratio measurements would decrease with this alternate cluster center definition, which would serve to strengthen our overall finding of the central location of high-flux cores.

REFERENCES

Allison, R. J., Goodwin, S. P., Parker, R. J., et al. 2009a, ApJL, 700, L99
Allison, R. J., Goodwin, S. P., Parker, R. J., et al. 2009b, MNRAS, 395, 1449
Allison, R. J., Goodwin, S. P., Parker, R. J., Portegies Zwart, S. F., & de Grijs, R. 2010, MNRAS, 407, 1098
Ascenso, J., Alves, J., & Lago, M. T. V. T. 2009, A&A, 495, 147
Berry, D. S. 2015, A&C, 10, 22
Billot, N., Schisano, E., Pestalozzi, M., et al. 2011, ApJ, 735, 28
Bonnell, I. A., & Davies, M. B. 1998, MNRAS, 295, 691
Bonnell, I. A., Vine, S. G., & Bate, M. R. 2004, MNRAS, 349, 735
Buckle, J. V., Curtis, E. I., Roberts, J. F., et al. 2010, MNRAS, 401, 204
Carpenter, J. M., Meyer, M. R., Dougados, C., Strom, S. E., & Hillenbrand, L. A. 1997, AJ, 114, 198
Cartwright, A., & Whitworth, A. P. 2004, MNRAS, 348, 589
Cartwright, A., & Whitworth, A. P. 2009a, MNRAS, 392, 341
Cartwright, A., & Whitworth, A. P. 2009b, A&A, 503, 909
Casertano, S., & Hut, P. 1985, ApJ, 298, 80
Chapin, E. L., Berry, D. S., Gibb, A. G., et al. 2013, MNRAS, 430, 2545
Conover, W. J. 1999, Practical Nonparametric Statistics (3rd ed.; New York: Wiley)
Csengeri, T., Bontemps, S., Schneider, N., Motte, F., & Dib, S. 2011, A&A, 527, A135
Currie, M. J., Berry, D. S., Jenness, T., et al. 2014, in ASP Conf. Ser. 485, Astronomical Data Analysis Software and Systems XXIII, ed. N. Manset, & P. Forshay (San Francisco, CA: ASP), 391
Davidge, T. J. 2012, ApJ, 761, 155
Davidge, T. J. 2015, ApJ, 799, 97
Ellerbroek, L. E., Bik, A., Kaper, L., et al. 2013, A&A, 558, A102
Elmegreen, B. G., Hurst, R., & Koenig, X. 2014, ApJL, 782, L1
Enoch, M. L., Evans, N. J., II, Sargent, A. I., et al. 2008, ApJ, 684, 1240
Evans, N. J., II, Dunham, M. M., Jørgensen, J. K., et al. 2009, ApJS, 181, 321
Feigelson, E. D., Townsley, L. K., Broos, P. S., et al. 2013, ApJS, 209, 26
Foster, J. B., Cottaar, M., Covey, K. R., et al. 2015, ApJ, 799, 136
Foster, J. B., Rosolowsky, E. W., Kauffmann, J., et al. 2009, ApJ, 696, 298
Friesen, R. K., Di Francesco, J., Shirley, Y. L., & Myers, P. C. 2009, ApJ, 697, 1457
Gennaro, M., Brandner, W., Stolte, A., & Henning, T. 2011, MNRAS, 412, 2469
Girichidis, P., Federrath, C., Allison, R., Banerjee, R., & Klessen, R. S. 2012, MNRAS, 420, 3264
Gomez, M., Hartmann, L., Kenyon, S. J., & Hewett, R. 1993, AJ, 105, 1927
Gouliermis, D., Keller, S. C., Kontizas, M., Kontizas, E., & Bellas-Velidis, I. 2004, A&A, 416, 137
Gutermuth, R. A., Megeath, S. T., Myers, P. C., et al. 2009, ApJS, 184, 18
Hatchell, J., Fuller, G. A., Richer, J. S., Harries, T. J., & Ladd, E. F. 2007, A&A, 468, 1009
Heiderman, A., & Evans, N. J., II 2015, ApJ, 806, 231
Hillenbrand, L. A., & Hartmann, L. W. 1998, ApJ, 492, 540
Holland, W. S., Bintley, D., Chapin, E. L., et al. 2013, MNRAS, 430, 2513
Hunter, T. R., Brogan, C. L., Cyganowski, C. J., & Young, K. H. 2014, ApJ, 788, 187
Hunter, T. R., Brogan, C. L., Megeath, S. T., et al. 2006, ApJ, 649, 888
Johnstone, D., Fich, M., Mitchell, G. F., & Moriarty-Schieven, G. 2001, ApJ, 559, 307
Jørgensen, J. K., Johnstone, D., Kirk, H., et al. 2008, ApJ, 683, 822
Jørgensen, J. K., Johnstone, D., Kirk, H., & Myers, P. C. 2007, ApJ, 656, 293
Kirk, H., Di Francesco, J., Johnstone, D., et al. 2016, ApJ, 817, 167 (K16)
Kirk, H., Johnstone, D., & Tafalla, M. 2007, ApJ, 668, 1042
Kirk, H., & Myers, P. C. 2011, ApJ, 727, 64 (KM11)
Kirk, H., & Myers, P. C. 2012, ApJ, 745, 131
Kirk, H., Offner, S. S. R., & Redmond, K. J. 2014, MNRAS, 439, 1765
Kirk, J. M., Ward-Thompson, D., & André, P. 2005, MNRAS, 360, 1506
Könyves, V., André, P., Men'shchikov, A., et al. 2015, A&A, 584, A91
Krumholz, M. R., Bate, M. R., Arce, H. G., et al. 2014, Protostars and Planets VI, ed. H. Beuther et al. (Tuscon, AZ: Univ. of Arizona Press), 243
Krumholz, M. R., Klein, R. I., & McKee, C. F. 2007, ApJ, 656, 959
Kryukova, E., Megeath, S. T., Gutermuth, R. A., et al. 2012, AJ, 144, 31
Kuhn, M. A., Feigelson, E. D., Getman, K. V., et al. 2014, ApJ, 787, 107
Lada, C. J., & Lada, E. A. 2003, ARA&A, 41, 57
Lada, E. A., Bally, J., & Stark, A. A. 1991, ApJ, 368, 432
Landsman, W. B. 1993, in ASP Conf. Ser. 52, Astronomical Data Analysis Software and Systems II, ed. R. J. Hanisch, R. J. V. Brissenden, & J. Barnes (San Francisco, CA: ASP), 246
Larson, R. B. 1995, MNRAS, 272, 213
Lombardi, M., Bouy, H., Alves, J., & Lada, C. J. 2014, A&A, 566, A45
Mairs, S., Johnstone, D., Kirk, H., et al. 2015, MNRAS, 454, 2557
Mairs, S., Johnstone, D., Kirk, H., et al. 2016, MNRAS, submitted
Maruta, H., Nakamura, F., Nishi, R., Ikeda, N., & Kitamura, Y. 2010, ApJ, 714, 680
Maschberger, T., & Clarke, C. J. 2011, MNRAS, 416, 541
Masiunas, L. C., Gutermuth, R. A., Pipher, J. L., et al. 2012, ApJ, 752, 127
Megeath, S. T., Gutermuth, R., Muzerolle, J., et al. 2012, AJ, 144, 192
Megeath, S. T., Wilson, T. L., & Corbin, M. R. 2005, ApJL, 622, L141
Meyer, M. R., Flaherty, K., Levine, J. L., et al. 2008, in Handbook of Star Forming Regions, Vol. 1, ed. B. Reipurth (San Franciso, CA: ASP Monograph Publications), 662
Moeckel, N., & Bonnell, I. A. 2009, MNRAS, 400, 657
Myers, A. T., Klein, R. I., Krumholz, M. R., & McKee, C. F. 2014, MNRAS, 439, 3420
Myers, P. C. 2011, ApJ, 743, 98
Palau, A., Fuente, A., Girart, J. M., et al. 2013, ApJ, 762, 120
Parker, R. J., Bouvier, J., Goodwin, S. P., et al. 2011, MNRAS, 412, 2489
Parker, R. J., Dale, J. E., & Ercolano, B. 2015, MNRAS, 446, 4278
Parker, R. J., & Goodwin, S. P. 2015, MNRAS, 449, 3381
Parker, R. J., Maschberger, T., & Alves de Oliveira, C. 2012, MNRAS, 426, 3079
Parker, R. J., Wright, N. J., Goodwin, S. P., & Meyer, M. R. 2014, MNRAS, 438, 620
Parmentier, G., Pfalzner, S., & Grebel, E. K. 2014, ApJ, 791, 132
Pattle, K., Ward-Thompson, D., Kirk, J. M., et al. 2015, MNRAS, 450, 1094
Pfalzner, S., & Kaczmarek, T. 2013, A&A, 559, A38
Porras, A., Christopher, M., Allen, L., et al. 2003, AJ, 126, 1916
Salji, C. J., Richer, S., Buckle, J. V., et al. 2015, MNRAS, 449, 1769
Seo, Y. M., Shirley, Y. L., Goldsmith, P., et al. 2015, ApJ, 805, 185
Simon, M. 1997, ApJL, 482, L81
Stolte, A., Brandner, W., Brandl, B., & Zinnecker, H. 2006, AJ, 132, 253
Stutz, A. M., Tobin, J. J., Stanke, T., et al. 2013, ApJ, 767, 36
Tafalla, M., Kumar, M. S. N., & Bachiller, R. 2006, A&A, 456, 179
Tan, J. C., Krumholz, M. R., & McKee, C. F. 2006, ApJL, 641, L121
Teixeira, P. S., Lada, C. J., Young, E. T., et al. 2006, ApJL, 636, L45
Wang, S., Looney, L. W., Brandner, W., & Close, L. M. 2008, ApJ, 673, 315
Ward-Thompson, D., Di Francesco, J., Hatchell, J., et al. 2007, PASP, 119, 855
Wright, N. J., Parker, R. J., Goodwin, S. P., & Drake, J. J. 2014, MNRAS, 438, 639
Zhang, Q., Wang, K., Lu, X., & Jiménez-Serra, I. 2015, ApJ, 804, 141